LUND UNIVERSITY

On microchannel acoustophoresis - Experimental considerations and life science applications

Augustsson, Per

2011

[Link to publication](#)

Total number of authors:
1

On microchannel acoustophoresis

*Experimental considerations and
life science applications*

Per Augustsson

Doctoral thesis, December 2, 2011

Public defence
December 2, 2011, 10.15 in E:1406, E-huset, LTH, Lund University
Ole Römers väg. 3, 223 63, Lund
http://www.elmat.lth.se/

Advisors
Prof. Thomas Laurell and Assoc. Prof. Johan Nilsson
Department of Measurement Technology and Industrial Electrical Engineering, Lund University

Faculty opponent
Assoc. Prof. Joel Voldman
Department of Electrical Engineering and Computer Science Massachusetts Institute of Technology, Cambridge, MA, USA

Board of examination
Prof. Tapio Visakorpi
Institute of Biomedical Technology, University of Tampere, Finland
Assoc. prof. Martin Wiklund
KTH, Applied Physics, AlbaNova University Center, Stockholm
Assoc. prof. Jonas Tegenfeldt
Department of Solid State Physics, Lund University
Deputy member: Stefan Andersson-Engels
Physics Department, Division of Atomic Physics, Lund University

Cover illustration
Microparticles moving in an ultrasound standing wave field. Image sequence overlay.

To the very last minute

Abstract

This thesis presents experimental studies of microchannel acoustophoresis, a technique for manipulation of microscopic objects in suspension by means of acoustic radiation forces induced by ultrasonic standing wave fields. By arranging an acoustic resonance across the width of a microchannel, the path of individual cells or microparticles can be deflected orthogonally to the fluid flow.

The propagation of acoustic waves in a microchip is discussed and a theory for the acoustic eigenmodes within the fluid filled channel is presented. With the intention to derive the trajectories of particles, expressions are recapitulated for the acoustic radiation force exerted on a particle in an acoustic field, the induced acoustic streaming in the fluid, and for the microchannel flow velocity profile. The introduced transport phenomena are thereafter used for evaluation of merits and limitations in microchannel acoustophoresis separating systems.

In five studies, microchannel acoustophoresis has been adapted for applications in life science. Three of these relate to sample preparation through transfer of cells and microparticles from one suspending fluid to another, for bead based bio-affinity assays, or cell suspension conditioning. A fourth study addresses on-chip elution of surface bound molecules from cells and microparticles. In study five, a system is described for pre-alignment and subsequent separation of cancer cells from blood cells based on their intrinsic acoustic and morphological properties.

In study six, a method is presented for measurement of the acoustophoretic velocity field of microparticles. This was done to test the extent to which the resonances in an acoustophoresis microchannel are well described by the current model.

i

List of papers

I. **Acoustic microfluidic chip technology to facilitate automation of phage display selection**
J. Persson, P. Augustsson, T. Laurell, and M. Ohlin
FEBS Journal, 275(22):5657–5666, 2008.

II. **Decomplexing biofluids using microchip based acoustophoresis**
P. Augustsson, J. Persson, S. Ekström, M. Ohlin, and T. Laurell
Lab Chip, 9(6):810–818, 2009.

III. **Buffer medium exchange in continuous cell and particle streams using ultrasonic standing wave focusing**
P. Augustsson, L. B. Åberg, A M. K. Swärd-Nilsson, and T. Laurell
Microchim Acta, 164(3-4):269–277, 2009.

IV. **Microfluidic chip for sequential elution of peptides from beads or cells allowing for investigation of surface bound molecules**
P. Augustsson, J. Malm, and S. Ekström
(manuscript)

V. **Label free cancer cell enrichment from blood samples exploiting acoustophoretic properties of cells**
P. Augustsson[†], C. Magnusson[†], M. Nordin, H. Lilja, and T. Laurell
(manuscript)

VI. **Automated and temperature-controlled micro-PIV measurements enabling long-term-stable microchannel acoustophoresis characterization**
P. Augustsson[†], R. Barnkob[†], S. Wereley, H. Bruus, and T. Laurell, *Lab Chip*, DOI: 10.1039/C1LC20637K, 2011.

[†] Authors 1 and 2 share first authorship

iv

Preface

This thesis summarizes the main part of my work at the Department of Measurement Technology and Industrial Electrical Engineering dating back to 2006. Six papers are included in the thesis, four of these are published (I-III and VI), and two are manuscripts (IV and V). These report, with one exception, paper VI, feasibility studies of microchannel acoustophoresis in life science applications. Paper VI presents a measurement system for assessment of acoustophoretic velocity fields.

Firstly I would like to recommend those readers that are not so familiar with subjects such as sound, microchannels, and life science, to begin by reading chapters 7 and 8. These are written in Swedish and presents the subject of this thesis in a simple form. (Kapitel 7 och 8 är polulärvetenskaplig bakgrund respektive sammanfattning på svenska.)

The first chapter of the introductory part of the thesis presents microchannel acoustophoresis and gives an overview of the history of the research field. Also, the papers are briefly introduced, and the reader can thereafter choose either to proceed by reading the papers (I-V), or by reading the theory chapter 2 that covers most of the relevant equations in microchannel acoustophoresis. In chapter 3, on separation, merits and limitations of microchannel acoustophoresis are evaluated by exploring many of the phenomena that may affect separation outcome. When possible, figures of merits are given and relations are derived. To say the least, paper VI is very rich on information. In chapter 4 is therefore given a condensed version of that paper which have bearing on the preceding chapters. Those readers interested in the details and aspects of the implementation of microchannel acoustophoresis platforms are referred to chapter 5.

I would like to thank the following persons:
My supervisor Thomas Laurell, for giving me the opportunity to play around for so many years. And for paying me to do it. My supervisor and chief Johan Nilsson for taking part in that, and for still remembering how electronic circuits works. Dr. and banker Filip Petersson, who skilfully lured me in to this institution in the first place. Keep luring.

Contents

Contents

1

Microchannel acoustophoresis

This chapter gives an overview of microchannel acoustophoresis. After a brief introduction of the general concept, the history of the research field is outlined in a rather selective manner so as to arrive at the topic of this thesis. Thereafter the included publications are introduced.

1.1 Introduction

The term microchannel acoustophoresis normally refers to a system designed to translate particles[1] suspended in a fluid by means of acoustic radiation forces in a continuous flow microchannel. The goal is to deflect the particles paths relative to the suspending fluid (commonly referred to as carrier fluid) by imposing on them an acoustic force potential directed perpendicular to the microchannel flow, **Fig. 1.1**(**a**). The acoustic radiation force on a particle stems from a local distortion in a resonant sound field due to scattering from the particle. The motive for setting up these systems can be to enrich particles, to clarify[2] a suspension, to transfer particles from one carrier fluid to another, or to separate particles of different types based on their intrinsic acoustic properties and morphology, **Fig. 1.1**(**b**)-(**d**).

---

[1] particle – a microscopic object, a cell, or a microbead (in this thesis)
[2] clarify – to remove solids
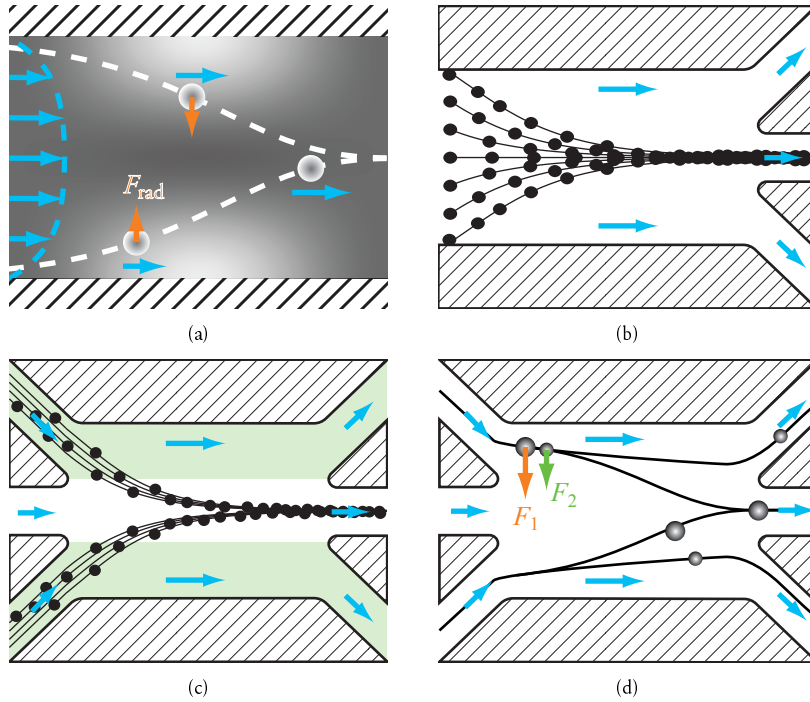
Figure 1.1: (**a**) Shows a schematic of the trajectories of particles subjected to acoustic radiation forces in a microchannel flow. The acoustic radiation force $\boldsymbol{F}_{\mathrm{rad}}$ translate the particles towards the centre of the flow. The force potential field is indicated in grey levels. (**b**) Up concentration of particles by forcing particles to to a confined region of the flow and thereby also clarifying the carrier fluid near the walls. (**c**) Buffer exchange of particles by translation from one carrier fluid (green) to another (white). (**d**) Separation of particles based on differences in size, shape, and acoustic proprerties.

The acoustic radiation force

Essential for an acoustophoresis microchannel is the establishment of an acoustic resonance that interact with particles to induce motion relative to the carrier fluid. This can be achieved by vibrating the whole microchip device, **Fig. 1.2(a)**, and thereby create resonance patterns of sound within the fluid contained in the microchannel. A particle subjected to this resonant pressure field will experience a force in the direction of the acoustic pressure gradient, transferring the particle to either a point of minimal pressure variations, or, under some conditions, to a pressure maxima, **Fig. 1.2(b)** and (**c**). Acoustic radiation forces are present when the acoustic properties of the particle do not exactly match the acoustic properties of the suspending fluid. This mismatch causes a local distortion in the sound field due to scattering from the particle. The distortion results in a time averaged pressure difference on the surface of the particle that govern its motion.

(a)

(b)   (c)   (d)
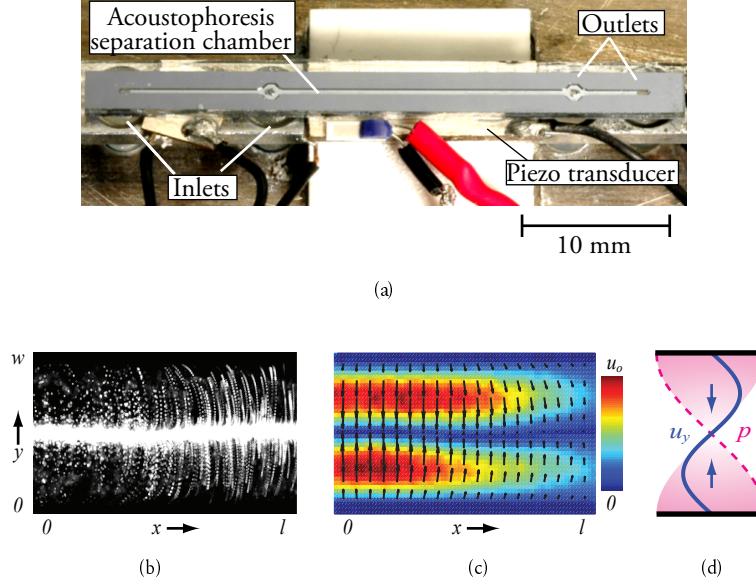
Figure 1.2: **(a)** Photo of an acoustophoresis device. A piezoelectric ceramic transducer underneath the chip vibrates the whole structure to induce acoustic resonances inside the channel. **(b)** Image sequence overlay of particles moving transversely in a segment of an acoustophoresis channel ($l \approx 1$ mm and $w \approx 375$ µm). The flow in the channel was temporarily stopped before the onset of sound. **(c)** The acoustophoretic velocity field of microbeads as measured by particle imaging velocimetry, along a 1 mm long section of the channel. Velocity magnitude and direction are indicated by colour and arrows, respectively. **(d)** The acoustophoretic velocity of microbeads u_y varies sinusoidally over the width of the channel and is period doubled with respect to the time harmonic acoustic pressure field p.

The acoustic resonance agglomerate particles along a central nodal line in the channel, **Fig. 1.2(b)**. In this configuration, the frequency f of the acoustic transducer have been chosen to fulfil the condition that the channel width w should be a multiple of half the acoustic wavelength λ

$$\lambda = \frac{2w}{n}, \qquad n = 1, 2, ... \qquad (1.1a)$$

$$f = \frac{c_o}{\lambda} = \frac{c_o n}{2w}, \qquad n = 1, 2, ... \qquad (1.1b)$$

where c_o is the speed of sound in the fluid, e.g. 1488 m s^{-1} for water at room temperature. In this thesis, most channels are of a with $w = 375$ µm in order to encompass a half wavelength standing wave at a driving frequency $f = 2$ MHz. Notably, the acoustophoretic velocity field varies also along the length of the channel, **Fig. 1.2(c)**. It will be shown

in chapter 2 that a 2- or 3-dimensional box potential may constitute a valid model of the acoustic resonances. This simplified model will be challenged in chapter 4 revealing that in experimental reality the resonance patterns are more complex than so. For design purposes, however, a plane wave approximation is reasonable, since in most applications, particles experience an acoustic field average along the whole length of the channel, that is clearly sinusoidal.

The acoustic radiation force on a particle is a complex function of its volume, acoustic properties relative to the suspending fluid, and the acoustic pressure field. The force on a particle is counteracted by friction from the suspending fluid which introduces a size and shape dependency for the motion path of the particle. **Table 1.1** list acoustofluidic[3] parameters and their general effect on the acoustophoretic focusing rate of a particle. Notably, the force need not necessarily be directed towards the channel centre. Some particles, typically fat or oil droplets, move towards the walls and are said to have negative acoustic contrast. In chapter 2 the acoustophoretic contrast factor is described in more detail.

Property	Acoustophoretic focusing rate
Size (a)	↗
Density (ρ_p)	↗
Compressibility (κ_p)	↘
Shape	?

Table 1.1: Acoustophysical properties and their general effect on the acoustophoretic focusing rate. ρ_p and κ_p are density and compressibility of the particle, respectively. Note, that the focusing rate can be negative for low density and/or high compressibility.

1.2 Historic review

This is a short review of the main landmarks of microchannel acoustophoresis dating back more than a century. It should be noted that much has been left out due to the narrow scope of this thesis.

The earliest reported observation of motion of particles in acoustic standing wave fields was that of August Kundt (1839-1894) and dates back to 1866 [2]. By studying the motion of dust particles in a column of gas brought into acoustic resonance, he could conclude that minute particles tend to agglomerate in the pressure nodes of resonant sound fields. This so called Kundt's tube was demonstrated for measurement of the speed of sound in various gases, and later also in liquids [3].

Kundt was inspired by the so called Chladni plate [4], which is a vibrating plate with sand on it. The vibrations cause the sand particles to reorganize according to the

---

[3] acoustofluidics – application of acoustic pressure fields in microfluidic systems [1]

resonant modes of the plate, **Fig. 7.1**. The subtle but significant difference between the two experiments is that in Chladni's experiment the particles interact with the transverse motion of the vibrating plate, while in a Kundt's tube interaction occur between a particle and the longitudinal vibrations of a fluid. Nothing was, even then, new under the sun, for Hooke had reported something similar to Chladnis experiment already in 1680, using a glass plate and a bow.

Later it was discovered that two types of motion are involved when bringing these systems into resonances. One is the above mentioned accumulation of particles in the pressure nodes, which is indicative of a force potential. The other observed motion was that of very minute particles that seemed to move in a steady current, which is typically a streaming phenomena. This was reported by Faraday [5], Savart (currents on Chladni plate), and Dvorak (currents in Kundt's tube).

These streaming phenomena very much interested Lord Rayleigh, especially the observation of Savart, that the streaming phenomena was not observed for a Chladni plate in vacuum. To Rayleigh it was clear that the streaming must be associated with energy dissipation, i.e. friction, in the air boundary layer near the surface of the plate. So he put forward a theory for this in 1884 [6]. It will be evident that this so called Rayleigh streaming is highly relevant for the work presented in this thesis.

The theoretical studies of acoustic radiation forces on particles have a somewhat shorter history. In 1934, King derived the acoustic radiation pressure on an incompressible sphere [7]. Short thereafter his results were used by Klein [8] to measure sound radiation intensity by monitoring the motion of a metal sphere suspended in a torsion pendulum. King did probably not at this stage envision acoustic radiation forces to be used for miniaturized cell handling, and any effect of compressibility of the sphere was left out.

In 1955, Yosioka and Kawasima [9] derived the acoustic radiation force on a compressible sphere, a derivation that was summarized and generalized by Gorkov [10] in 1962. The extension of the theory to compressible spheres was a significant improvement as it allows for calculation of the force exerted on polymer particles, droplets, and microorganisms. Doinikov [11] suggested that the viscous boundary layer surrounding a particle impact the acoustic radiation force. In a very recent paper, Setnes and Bruus [12] carried out calculations for this so called viscous boundary layer correction.

Experimentalists rediscovered the acoustic radiation force in 1971. Dyson *et al.* reported the discovery of blood cell banding in vessels in chick embryos when exposed to an ultrasonic beam [13]. In this short communication, containing no references to previous work on radiation forces, Bernoulli attraction was hypothesized to govern the motion of blood cells. Baker picked up on this blood cell banding and reported that the sedimentation rate of blood cells can be increased by exposure to a resonant acoustic field [14] and could rule out Bernoulli attraction, but did not give any alternative explanation. Interestingly, the acoustic intensities in the experiments was measured using a swinging ball radiation balance, very much similar to that presented by Klein in 1938 for which King had derived his theory.

In the past two decades ultrasound standing waves for particle manipulation and sep-

5

aration has received renewed interest since the early papers of Mandralis and Feke [15, 16] who introduced half wavelength acoustic resonators, followed by Yasuda *et al.* [17], and Hawkes and Coakley [18, 19] who initiated the transition to a microscale format. The first microfabricated silicon/glass acoustic resonator was presented by Harris *et al.* in 2003 [20].

Up until 2002 all half wavelength resonators were flat, in the sense that the resonance condition was fulfilled for the smallest dimension of a cavity. Nilsson *et al.* (a.k.a. Lenshof) was first to demonstrate acoustic control of particles in standard wet etched rectangular cross section silicon glass microchannels [21, 22]. The configuration, maintaining a resonance in the width dimension of such channels, presents improved flexibility in routing of channels, splitting of flow streams, and ease of visualization, since the acoustic motion of particles is orthogonal to the glass surface sealing the channel. To distinguish the device category from the earlier parallel plate geometries, the term transverse mode acoustophoresis has been proposed. Petersson *et al.* applied the technique to the separation of fat particles from blood [23], fluid exchange of suspended particles [24] and size sorting of particles and cells [25]. Aspects of cell viability in such channels have been studied by Svennebring *et al.* [26] and more recently by Dykes [27]. Manneberg *et al.* have investigated the use of multiple transducers on a single device [28] and so has Adams [29], who also combined acoustic and magnetic forces on a single device [30].

In this thesis, the term *microchannel acoustophoresis* refers to this type of separation devices having primarily a resonance across the width of the channel.

1.3   Summary of the papers

The foundation of this thesis are the 6 papers that can be found at the end of this book. In this section, each paper is introduced briefly, focusing not necessarily on the technical aspects of acoustophoresis but rather on the underlying motive behind the work. Admittedly though, in most of the papers the technical aspects coincide with the underlying motives. In all the reported work, I have constructed the acoustophoresis chip, put together the experimental setup and run the samples in the device. I have taken a significant part in the experimental planning and in the interpretation of the results. I have taken part in writing all of the manuscripts and I have produced most of the experimental drawings.

Paper I: Acoustic microfluidic chip technology to facilitate automation of phage display selection

In this paper, microchannel acoustophoresis was applied for automated affinity selection and enrichment of specific binders (e.g. antibodies) from phage[4] display libraries. Such binders will e.g. allow for assessment of all components of the proteome, an approach important for efficient diagnosis, prediction and treatment of disease. Phage display [31]

---

[4] bacteriophage – A viral particle, that reproduce by infecting bacteria, and that can also present molecular material on its surface.

is a leading method for isolating new binders from molecular libraries containing large sets of related but different molecules.

Phage display is normally performed according to the following scheme. The target molecule (e.g. an antigen) is immobilized onto a surface, often in the form of a microbead. Following incubation in a phage library, phage viral particles that display on their surface different antigen-specific antibody fragments, will be caught on the antigen-coated surface. By washing away unbound phages, those phages displaying binders targeting the antigen are enriched and they can be used to produce the associated antibody fragments.

Current procedures are labour intense and require manual intervention, preventing high throughput approaches for development of specific binders by this technology. In an attempt to implement phage display selection in a microchannel acoustophoresis setting, a device for efficient washing of microbeads was developed and demonstrated for selection of binders targeting a grass pollen allergen. For comparison, the same procedure was carried out in parallel for a manual protocol involving centrifugation and magnetic capture of phage-laden microbeads.

The input sample mixture was a suspension of allergen-coated microbeads that had been incubated with a phage library. The suspension was introduced along the side walls of an acoustophoresis channel while particle free buffer was injected through a central inlet. As the microbeads flowed through the channel, the acoustic radiation force directed them towards the central outlet of the channel. Phages that did not bind to the surface of a microbead was not subjected to any significant acoustic radiation force due to their minute size, and would therefore exit through the side outlets, **Fig. 1.3**.
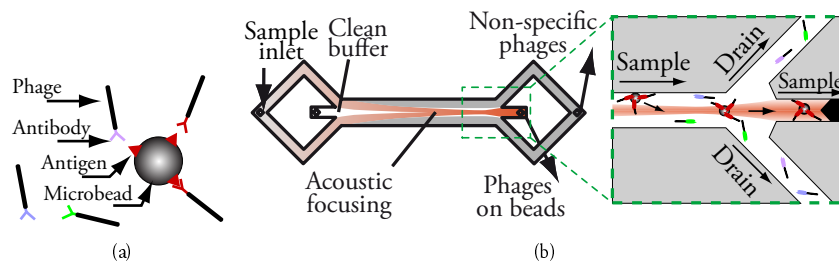
Figure 1.3: **(a)** Phages were incubated with allergen-coated microbeads. Those phages displaying antibodies that matched the target allergen, bound the beads. **(b)** Schematic of the acoustophoresis microchip. Microbeads, carrying bound phages, are focused to the centre of a microchannel by the acoustic radiation force. Phages that are not bound to a microbead exit through the side outlets.

Microchannel acoustophoresis for carrier fluid exchange of cells was first presented by Hawkes [32], **Fig. 3.1(b)**. In this work, however, a device similar in design to that of Petersson *et al.* [24] was developed. In order to achieve sufficient washing efficiency, the device performs two sequential cycles of fluid exchange. The presented two step acoustic extraction of phages displayed thousand fold enrichment of phages displaying specific

binders as compared to input sample.

Paper II: Decomplexing biofluids using microchip based acoustophoresis

This work was in a sense a prequel to paper I, in that the very same acoustophoresis chip was evaluated in terms of washing efficiency. In another aspect, it was an advancement since the method was applied for mass spectrometry sample preparation with some success.

The washing efficiencies of paper I were considerably much higher than what could be expected based on previous work by Petersson *et al.* [24], even taking into account the sequential wash strategy. Therefore a number of experiments were carried out to find what physical parameters could explain the discrepancy in the experimental outcome.

It was concluded that the washing efficiency was highly influenced by the concentration of microbeads in the suspension. For low concentrations of beads, the contamination after wash was found to be proportional to the number of beads in the inlet suspension. For higher bead concentrations, however, the washing efficiency per bead can be expected to decrease dramatically. For high concentrations, the average distance between beads becomes small and contaminant is convected to the central outlet through viscous interactions. The implication of this is important because it imposes a limitation to the technique. For high concentrations of particles, such as whole blood, precision will inevitably be poor. This phenomenon, which is of course not by any means restricted to microchannel acoustophoresis, is discussed in greater detail in section 3.1.

Paper III: Buffer medium exchange in continuous cell and particle streams using ultrasonic standing wave focusing

A new strategy was proposed in this work, to address carrier fluid exchange of particle rich suspensions. Rather than transporting the particles across a boundary between two fluids, the particles are confined in the centre of the channel by the ultrasound, whereafter the initial medium is removed and new medium is added. In a sense it is similar to manual centrifuge based washing where particles are first confined to the bottom of a test tube by centrifugation and thereafter the supernatant is removed and exchanged with new fluid.

Fig. 1.4 shows a schematic of the method. Particles are initially focused to the centre of an acoustophoresis pre-alignment channel, depleting the regions of the flow near the channel walls. At a first intersecting flow junction, a fraction of the main channel flow is extracted on one side of the channel while new carrier fluid is injected on the opposing side. After escaping this flow junction, particles are re-focused to the centre of the main channel flow. The process of shifting new medium into the main channel is then repeated in sequence of consecutive flow junctions.

In summary, it was concluded that the device displayed improved ability regarding washing efficiency for suspensions of microbeads and red blood cells at concentrations up to $2\%_{vol}$. The improvement was however not as pronounced as might have been expected. One explanation to this is that once particles are brought in close proximity, they tend
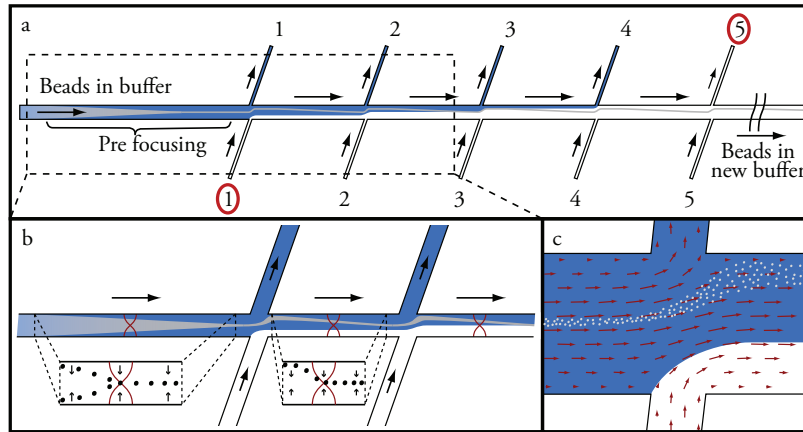
Figure 1.4: Principle of operation for sequential side shifting, presented in papers III and IV. Reproduced from paper III, with kind permission from Springer Science+Business Media.

to move as one entity rather than as individual particles. Contaminant molecules can be encapsulated inside this elongated cluster and will thus follow the stream of particles through the separation channel.

Paper IV: Microfluidic chip for sequential elution of peptides from beads or cells allowing for investigation of surface bound molecules

An interesting feature of the above presented platform, is the ability to address all the flow junctions individually. Rather than performing repeated exchange of a single buffer in all the flow junctions, the chip was used for sequential treatment of cells and microbeads in different buffer conditions.

The motive for performing such sequential buffer exchange was to isolate loosely bound proteins and peptides from the surface of beads and cells. By exposing beads or cells to a sequence of different buffer conditions, in the form of a pH-gradient, peptides and proteins were eluted off the surface based on PI. The side outlets to the chip was sampled, each containing the molecules eluted off the surface of cells at a specific stage in the buffer sequence. Collected side outlet fractions were purified using solid phase extraction and analysed with MALDI-MS. The device was successfully applied for wash and sequential elution of peptides bound to the surface of microbeads and human spermatozoa.

Paper V: Label free cancer cell enrichment from blood samples exploiting acoustophoretic properties of cells

The purpose of this project, that aims at clinical application, was to separate cancer cells from samples of blood.

Circulating tumour cells (CTCs) are tumour cells circulating in the blood, which are shed from the primary tumour or its metastases [33]. CTCs can been found in the blood of patients with cancer of epithelial cell origin, having metastatic disease [34] but are extremely rare in healthy persons [35].

To date, most successful techniques to enrich CTCs from metastatic cancer patients depend on immuno-labelling [36] through the epithelial cell adhesion protein (EpCAM), that is expressed on the surface of a majority of epithelial tumour cells. Alternative methods for isolation of CTCs are currently being explored extensively. The reason for this is that CTCs display great variations in antigen expression and morphology which indicates that many cells may not be detectable using standard protocols.

In this project, acoustophoresis is proposed as a viable route to extract CTCs from blood. For this purpose, an acoustophoresis microchannel was developed that incorporate pre-alignment and subsequent separation of cells based on intrinsic acoustic and morphological properties. From previous work it had been concluded that cell number concentration is a limiting factor, so the blood was depleted of red blood cells (RBCs) through selective osmotic lysis prior to separation.

The expected number of CTCs in the input samples is extremely low compared to the levels of white blood cells (WBCs) present in the blood, which are to be considered a contamination in this context. The rareness of the CTCs is an enormous challenge for the separation system, and therefore reproducibility and precision were important aspects when designing the device.

Paper VI: Automated and temperature-controlled micro-PIV measurements enabling long-term-stable microchannel acoustophoresis characterization

The acoustic resonances in acoustophoresis microchannels are yet not fully understood. In chapter 2, a theoretical model is presented, for the acoustic field inside the acoustophoresis channel. In this model any influence from the surrounding chip material is disregarded. In the presented work the extent to which this simplification is valid was experimentally quantified. The study is summarized in chapter 4.

2

Theoretical models

This chapter presents the basic equations governing acoustophoresis. The theory for sound is not treated but can be studied in the textbooks by Lighthill [37], Pierce [38], and Bruus [1]. General microfluidics can be studied in various textbooks [1, 39–43]. An extensive review on the physics of microfluidics was written by Squires and Quake in 2005 [44].

There exist to date no experimentally verified integrated model for microchannel acoustophoresis that takes into account the coupling of sound from the piezo actuator into the silicon/glass structure of the chip and the water filled channel. The approach will rather be to discuss how vibrations propagate in the bulk of the chip, and thereafter introduce a simplistic model for the acoustic pressure field inside the channel, neglecting any interaction with the bulk. From the acoustic field, the acoustic radiation force on a compressible sphere can be derived which determine the acoustophoretic motion of particles. Acoustic streaming velocity is calculated, which is an important limiting factor in acoustophoresis. At the end of the section, particle trajectories are simulated, taking into account the microchannel velocity flow profile.

2.1 Sound propagation in the microchip

Fig. 2.1(a) shows a perspective view of an acoustophoresis microchannel in its most simple form, comprising a water-filled channel etched in silicon, a bonded borosilicate lid, and a piezo transducer. Throughout this thesis, the channel is always oriented along the x-axis. It is clear from the cross sectional view in **Fig. 2.1(b)** that the channel occupies only a tiny fraction of the total volume of the mechanical structure. The piezo has been placed underneath the chip and emits vibrations normal to the underside. A subject that has been under some debate is whether the angle of incidence of the sound, i.e. the orientation of the piezo, has any significant impact on the coupling efficiency of acoustic energy into the channel. Intuitively, it would be more effective to orient the transducer along the y-direction. To calibrate the intuition slightly, one can study the somewhat naive **Fig. 2.1(c)** showing the transient propagation of an acoustic impulse from a point source located on the underside of the chip. The wavelength $\lambda = c/f \approx 3$ mm in the borosilicate glass is of the same order as the chip dimensions. During the first period of an oscillation, the wave has already lost its initial orientation due to the finite geometry. Typically, an oscillation dies out in the system after $\sim$1000 cycles. In a glass device this would correspond to 2.5 m of propagation, hence, an oscillation would be reflected $\sim$1000 times before dying out. For increasing chip size and complexity the effect of the positioning of the transducer should decrease as more imperfections are introduced. Despite the many reflections, the positioning and the angle [45] of the transducer does have a very pronounced effect in experiments so a deeper understanding of the matter is desirable.
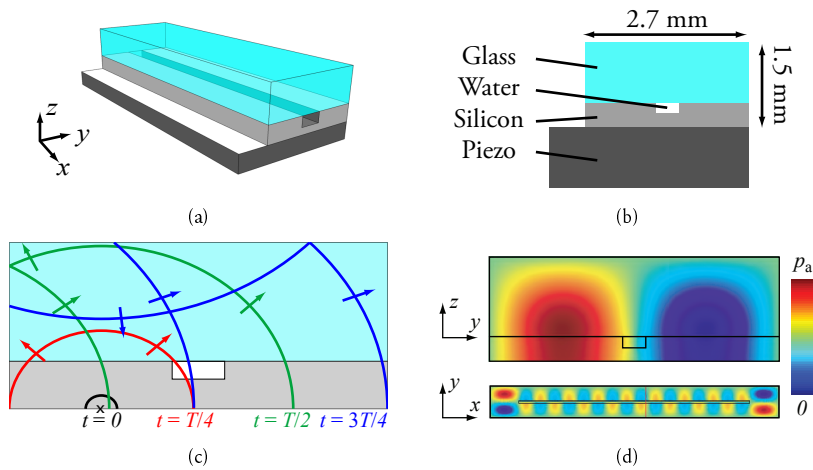
Figure 2.1: **(a)** Perspective, schematic view of an acoustophoresis chip and a piezo transducer. **(b)** Cross sectional view of the chip. **(c)** Schematic of a pressure impulse propagating in the transverse cross section of the chip, during the first period of oscillation ($t < T$). Multiple reflections are discarded. Inspiration from Hedberg, Master's thesis [46]. **(d)** Simulation results of the pressure field in the chip, from Barnkob Master's thesis [47]

2.2   Acoustic eigenmodes

The following two sections on the subject of acoustic resonance and acoustic radiation force, are to most part a summary based on derivations by Barnkob [48], Andersen *et al.* [49], and two tutorials on acoustofluidics by Henrik Bruus [50, 51]. Derivations were carried out for a compressible isothermal fluid by combining the thermodynamic equation of state expressing pressure p as a function of density ρ, the kinematic continuity equation for ρ, and the dynamic Navier-Stokes equation.

To calculate the acoustic eigenmodes inside the acoustophoresis channel, some simplifications are made. Any interaction with the chip material surrounding the channel is neglected and the walls confining the liquid inside the channel are considered acoustically hard. The water inside the acoustophoresis channel has lower density and is more compressible than the surrounding silicon walls. The difference in acoustic impedance of the water $Z_{\mathrm{wa}} = \rho_{\mathrm{wa}} c_{\mathrm{wa}} = 1.5\,\mathrm{MPa\,s\,m^{-1}}$ and the wall $Z_{\mathrm{si}} = \rho_{\mathrm{si}} c_{\mathrm{si}} = 20\,\mathrm{MPa\,s\,m^{-1}}$ cause $\sim 75\%$ of the incident acoustic energy to be reflected (see **Eq. 2.1**) upon each impact.

$$R = \left(\frac{Z_{\mathrm{si}} - Z_{\mathrm{wa}}}{Z_{\mathrm{si}} + Z_{\mathrm{wa}}} \right)^2 \approx 75\% \tag{2.1}$$

This implies that the simplifications above are reasonable, but it would come as no surprise if the acoustic field in the bulk outside the channel also influence the magnitude of the resonance inside the channel.

The channel forms an acoustic cuboid-shaped[1] cavity of length l, width w, and height h. Solutions are sought for the time-harmonic ultrasound pressure field $p_1 \exp(-\mathrm{i}\omega t)$ and velocity field $\boldsymbol{v}_1 \exp(-\mathrm{i}\omega t)$ where $\omega = 2\pi f$ is the angular frequency and f is the driving frequency. The complex time-harmonic notation is implicitly assumed in the following. The pressure eigenmodes can be found by looking for solution to the undamped Helmholtz wave equation (2.2) for a hard wall boundary condition.

$$4\nabla^2 p_1 = -k^2 p_1, \qquad \mathrm{BC}: \quad \boldsymbol{n} \cdot \boldsymbol{\nabla} p_1 = 0 \tag{2.2}$$

where $k = \frac{\omega}{c_0}$ is the wavevector and $\boldsymbol{n}$ is an outward pointing vector orthogonal to the wall and c_{wa} is the speed of sound in the liquid. It can be confirmed by substitution that

$$p_1(x,y,z) = p_{\mathrm{a}} \cos(k_x x)\cos(k_y y)\cos(k_z z), \qquad k_j = n_j \frac{\pi}{L_j} \tag{2.3}$$

is a solution to (2.2) where p_a is the pressure amplitude, $j = x,y,z$, $(L_x, L_y, L_z) = (l,w,h)$, and $n_j = 0,1,2,3\ldots$ is the number of half wavelengths along each direction. The resonances occur at frequencies

$$f_{n_x,n_y,n_z} = \frac{c_0}{2} \sqrt{\frac{n_x^2}{l^2} + \frac{n_y^2}{w^2} + \frac{n_z^2}{h^2}}. \tag{2.4}$$

---

[1] cuboid – a rectangular block

13

In all papers in this thesis $h < w = \lambda/2$ and therefore $n_z = 0$, which limits the number of dimensions to two. In this zero damping approximation the velocity field can be written

$$\boldsymbol{v}_1 = -\mathrm{i}\frac{\boldsymbol{\nabla}p_1}{\rho_\mathrm{o}\omega} = \mathrm{i}\frac{p_\mathrm{a}}{\rho_\mathrm{o}\omega}\left[\begin{array}{c} k_x\sin(k_xx)\cos(k_yy) \\ k_y\cos(k_xx)\sin(k_yy) \end{array}\right] \qquad (2.5)$$

where the imaginary unit (i) indicate a phase-shift of 90° between the maximal pressure and the maximal velocity. Energy is periodically converted between potential energy (stored as compression of fluid) and kinetic energy (the velocity field). Notably, the velocity is directed along the gradients of the pressure field, see **Fig. 2.2**. From the pressure field, the time-averaged acoustic energy density E_ac in the channel can be derived through

$$E_\mathrm{ac} = \frac{1}{4\rho_\mathrm{o}}\left[\frac{|\boldsymbol{\nabla}p_1|^2}{\omega^2} + \frac{p_1^2}{c_\mathrm{o}^2}\right]. \qquad (2.6)$$
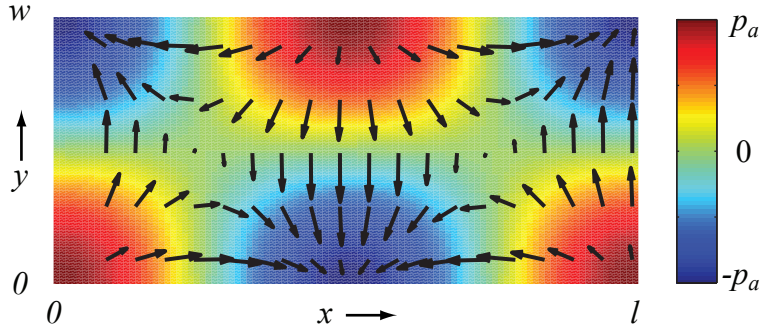
Figure 2.2: Plot of the acoustic field along x and y. The pressure field at time $t = 0$ is indicated by color, and the velocity field at time $t = T/4 = \pi/(2\omega)$ is indicated by arrows.

2.3   Acoustic radiation force

It has been mentioned already in section 1.2 that the most commonly referenced theory for the acoustic radiation force on a compressible sphere was presented by Gorkov [10]. His derivation starts from the following assumption: "The magnitude of the force is equal to the average flux of momentum through any closed surface in the fluid which encloses the particle." Upon incidence of a sound wave, the sphere will scatter and thereby interfere locally with the pressure field. Importantly, the wavelength is assumed to be much larger than the size of the particle. The sphere is compressed by the acoustic pressure field and oscillate back and forth in the acoustic velocity field.

For the scattering due to the compressibility, the sphere is treated as a monopole that reflect sound if the sphere is more rigid or softer than the surrounding fluid. The reflection arises because the radial motion of the surface of the sphere does not move in concert with the incoming wave. Similarly, reflection can occur due to density difference between the sphere and the fluid which lead to a phase shift between the oscillatory motion of the incoming wave and the motion of the sphere.

Gorkov calculated the resulting force on a suspended compressible sphere by summing up the two contributions to the average momentum flux through an infinitely large closed surface around the sphere.

General equations

Since the acoustic radiation force is caused by differences in acoustic properties between a particle (index p), and the suspending fluid (index o) it is convenient to introduce the ratios

$$\frac{c_\mathrm{p}}{c_\mathrm{o}} = \tilde{c}, \qquad \frac{\rho_\mathrm{p}}{\rho_\mathrm{o}} = \tilde{\rho}, \qquad \frac{\kappa_\mathrm{p}}{\kappa_\mathrm{o}} = \tilde{\kappa} \tag{2.7}$$

where c denotes speed of sound, ρ density, and $\kappa = 1/(c^2\rho)$ compressibility. Moreover, two coefficients are introduced

$$f_1 = 1 - \tilde{\kappa}, \qquad f_2 = \frac{2(\tilde{\rho} - 1)}{2\tilde{\rho} + 1} \tag{2.8}$$

that relates the contributions from the pressure field (f_1) and from the velocity field (f_2) to the acoustic force ($\boldsymbol{F}_\mathrm{rad}$) on the sphere.

$$\boldsymbol{F}_\mathrm{rad} = -\frac{4\pi a^3}{3}\left[f_1 \frac{\kappa_\mathrm{o}}{2} \boldsymbol{\nabla}\langle p_1^2 \rangle - f_2 \frac{3\rho_\mathrm{o}}{4} \boldsymbol{\nabla}\langle \boldsymbol{v}_1^2 \rangle \right] \tag{2.9}$$

where a is the particle radius.

Plane wave equations

For most purposes, a standing plane wave approximation of the acoustic radiation force is valid. From **Eq. 2.4** it is clear that if the frequency f is chosen such that $f = c_\mathrm{o}/\lambda = c_\mathrm{o}/(2w)$ then the number of periods along the length of the channel must be minimal. This implies that the pressure gradients along x are relatively small, whereby the force along x is negligible. Also, for continuous flow systems the variations along x cancels due to their periodic nature. For a half wavelength standing wave, the acoustic field reduces to

$$p_1 = p_\mathrm{a} \cos(k_y y) \tag{2.10a}$$

$$\boldsymbol{v}_1 = \mathrm{i}\frac{p_\mathrm{a}}{c_\mathrm{o}\rho_\mathrm{o}} \sin(k_y y)\boldsymbol{e}_y \tag{2.10b}$$

and the acoustic radiation force can be written

$$\boldsymbol{F}_{\mathrm{rad}} = 4\pi\,\Phi a^3 k_y E_{\mathrm{ac}}\sin(2k_y y)\boldsymbol{e}_y \tag{2.11a}$$

$$\Phi = \frac{f_1}{3} + \frac{f_2}{2} = \frac{1 - \tilde{\kappa}}{3} + \frac{2(\tilde{\rho} - 1)}{2\tilde{\rho} + 1} \tag{2.11b}$$

$$E_{\mathrm{ac}} = \frac{p_{\mathrm{a}}^2 \kappa_{\mathrm{o}}}{4} \tag{2.11c}$$

From (2.11a) it can be seen that the sign and magnitude of the force is dictated by the particles compressibility and density relative to the suspending medium. The force is zero in the center of the channel and at each wall, and maximal at $y = w/4$ and $y = 3w/4$. The acoustic contrast factor Φ can become negative, for particles of sufficiently low densities or high compressibility.

The motion of the particle relative to the suspending medium is retarded by a drag force (Stokes) such that

$$F_{\mathrm{rad}} = F_{\mathrm{drag}} = 6\pi a\eta u_{\mathrm{rad}} \tag{2.12}$$

where η is the dynamic viscosity and $urad$ is the velocity of the particle. Note the distinction between the time harmonic acoustic velocity field $\boldsymbol{v}_1$ and the various acoustofluidic velocities denoted $\boldsymbol{u}$, that will be introduced in the coming sections. For all relevant situations in this work, momentum of the particle can be neglected. From this force balance the velocity u_{rad} of the particle can be written

$$u_{\mathrm{rad}} = \frac{\mathrm{d}y}{\mathrm{d}t} = \frac{2\Phi}{3\eta} a^2 k_y E_{\mathrm{ac}}\sin(2k_y y) \tag{2.13a}$$

$$y(t) = \frac{1}{k_y}\arctan\left\{\tan\left[k_y y(0)\right]\exp\left[\frac{4\Phi}{3\eta}(k_y a)^2 E_{\mathrm{ac}}\,t\right]\right\}. \tag{2.13b}$$

where $y(t)$ is derived from u_{rad} by separation of variables y and t.

2.4 Acoustic streaming

The onset of an acoustic resonance will inevitably induce acoustic streaming in the channel. The streaming emanates from the thin viscous boundary layers at the top and bottom of the channel. For the plane wave velocity field $\boldsymbol{v}_1$ described in **Eq. 2.10b** the oscillatory velocity is maximal at the centre of the channel (i.e. for $y = w/2$), **Fig. 2.3**. In the bulk, the velocity field does not depend on z. At the boundary, near $z = 0$ and $z = h$ the velocity must, however, go to zero, so there must be a sharp velocity gradient normal to the boundary. Inside this thin boundary layer of thickness $\delta \approx 0.5$ µm, acoustic energy is converted to time independent convective recirculating flow. Due to the confined geometry and the symmetry in z, the streaming inside the boundary layer drives a current in the bulk of the fluid, as indicated in **Fig. 2.3**. The velocity field is a COMSOL simulation

based on the results of Lord Rayleigh for the boundary layer streaming induced by a plane standing wave propagating parallel to a rigid surface [6].

$$u_{\text{str}} = -\frac{3}{8}\frac{v_a^2}{c_o}\sin(2k_y y) = -\frac{3}{2}\frac{E_{\text{ac}}}{\rho_o c_o}\sin(2k_y y). \qquad (2.14)$$

Analytical solutions to acoustic streaming in a rectangular cross section microchannel can be studied in more detail in [52].
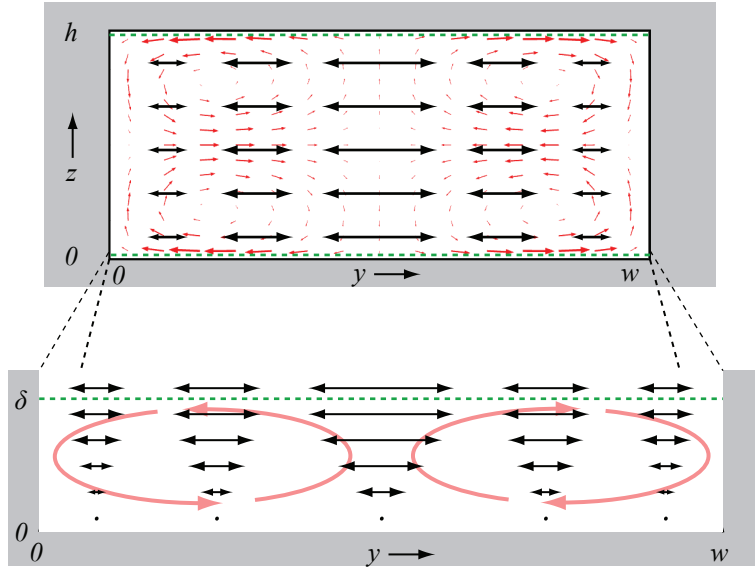
Figure 2.3: Acoustic streaming in the transverse cross section of the channel caused by the harmonically oscillating first order acoustic velocity field (black arrows). The lower part shows a blow up of the boundary layer of thickness δ (green dashed lines) and the steady second order streaming velocity field (red arrows).

A comparison of the magnitude of the streaming velocity u_{str} to the velocity of a particle due to acoustic radiation force u_{rad} yield

$$\frac{u_{\text{str}}}{u_{\text{rad}}} = \frac{9\eta}{8\pi\Phi a^2 \rho_o f} = \frac{9\eta w}{4\pi\Phi a^2 \rho_o c_o}. \qquad (2.15)$$

From **Eq. 2.15** it is possible to derive a critical radius a_c, for which $u_{\text{str}} = u_{\text{rad}}$. For particles smaller than this critical radius the streaming will dominate the motion and *vice versa*, given that the acoustic properties are identical. A polystyrene bead, in water, at $f = 2$ MHz, and at room temperature, has a critical radius $a_c = 1$ μm. For a polystyrene microbead of radius $a = 2.5$ μm suspended in water the streaming velocity magnitude is 15% of the acoustic radiation force. **Fig. 2.4** shows experimental images

from fluorescence-tagged lipo-proteins of radius $a \approx 50$ nm $<< a_c$, initially flow laminated along the sides of an acoustophoresis channel. The swirling motion is a function of acoustic streaming and the flow velocity profile in the channel.
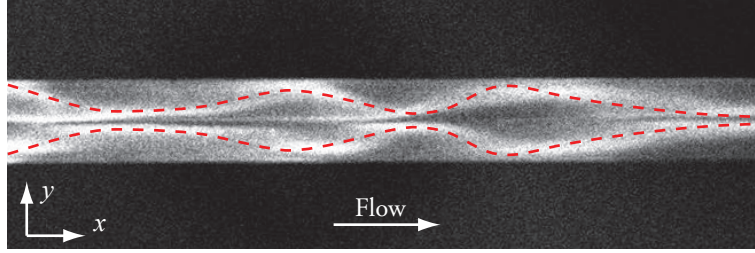
Figure 2.4: Lateral acoustic streaming of fluorescence tagged lipo-proteins in a continuous flow acoustophoresis microchannel. The swirling motion is indicated by red dashed curves. From Augustsson, Master's thesis [53].

For particles of $a > a_c$, the interplay between the acoustic streaming and the acoustic radiation force is intricate. At $z = h/2$, the direction of the two effects coincide while at $z = 0$ and $z = h$ the sign is opposite. At the onset of sound, particles migrate to the central nodal plane, but since the acoustic radiation force has no z-component in the plane wave assumption, the streaming will eventually transport all the initially focused particles to the channel ceiling or floor.

2.5   The Poiseuille flow profile

In microchannel flow, the velocity distribution in the transverse cross section is dominated by the zero-velocity condition at the channel walls. For a long channel, that is translationally invariant along the flow direction (x), the velocity $\boldsymbol{v}(\boldsymbol{r}) = v_x(y, z)\boldsymbol{e}_x$ Navier-Stokes equation becomes

$$\boldsymbol{0} = \eta \nabla^2 [v_x(y, z)\boldsymbol{e}_x] - \boldsymbol{\nabla} p \tag{2.16}$$

where $\boldsymbol{\nabla} p$ is a linearly decreasing volume force that is balanced by the friction force from the walls communicated to the fluid through viscosity η.

For a flow between two parallel plates, i.e. for high aspect ratio channels an analytical solution can be found for the flow profile.

$$v_x(z) = \frac{\Delta p}{2\eta l}(h - z)z \tag{2.17}$$

where Δp is the pressure drop over a channel segment of length (l) and height (h).

For a channel of rectangular cross section no analytical solution is known for the Poiseuille-flow profile. A solution can, however, be expressed as an infinite sum.

$$v_x(y) = \frac{4h^2 \Delta p}{\pi^3 \eta l} \sum_{n,\,\text{odd}}^{\infty} \frac{1}{n^3} \left[1 - \frac{\cosh\left(n\pi \frac{y - w/2}{h}\right)}{\cosh\left(n\pi \frac{w}{2h}\right)} \right] \sin\left(n\pi \frac{z}{h}\right) \qquad (2.18)$$

The sum converges fast, and for most cases only the first four terms are necessary to include. The function is plotted in **Fig. 2.5**.
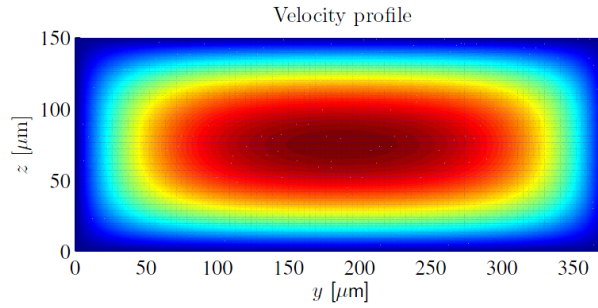
Figure 2.5: The Poiseuille velocity profile for microchannel flow in a rectangular geometry. The velocity u_x is zero (blue) at the boundaries and maximal (red) in the centre of the channel.

2.6 Particle paths

In the above sections, the velocity of a particle was derived for influence from the acoustic radiation force, the acoustic streaming velocity field, and the Poiseuille flow profile. In this section, the resulting particle trajectories are studied. Adhering to the plane wave approximation, i.e. when there is no acoustic wave component along the length of the channel, three effects come into play. Along the x-direction the velocity u_x^{P} is governed solely by the Poiseuille flow profile (**Eq. 2.18**). The velocity due to acoustic radiation force u_{rad} (**Eq. 2.13a**) act only along the y-direction, and the acoustic streaming u_{str} act orthogonal to the flow, in the yz-plane. By numerical simulation it is possible to visualize the path of a particle during a passage through an acoustophoresis channel. Acoustic streaming is disregarded herein, but can easily be incorporated in the simulation.

In **Fig. 2.6(a)** are shown trajectories for a particle for different initial positions along the width of the channel, and at $z = h/2$. From observing the distance Δy between adjacent trajectories it is apparent that the dispersion in y is small. Only for the outermost particle trajectories Δy increases slightly. Notably, a particle can never be closer to the wall than one radius, so the acoustic radiation force will be non-zero at the wall.

The initial z-position of particles impact their trajectories dramatically, **Fig. 2.6(b)**. This is attributed to the parabolic nature of the velocity distribution in the height domain.

19

Particles flowing near the top ($z = h$) or bottom ($z = 0$) reach the channel centre ($y = w/2$) at an earlier stage than do particles flowing at e.g. $z = h/2$. Particles that flow slowly in the x-direction spend more time in the acoustic field and are thereby moved into the centre at a shorter distance along x.

(a): $z = h/2$ (b): z range from 0 to h
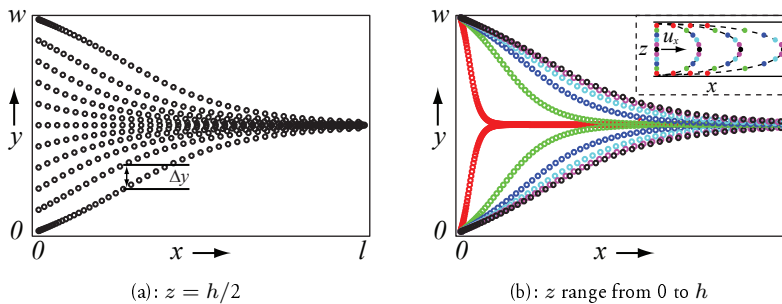
Figure 2.6: Simulated trajectories of 7 μm polystyrene particles in an acoustophoresis microchannel. (**a**) Particles initially at $z = h/2$ and distributed in y. Outermost particles start one particle radius away from the wall. (**b**) Particles initially at each wall and distributed in z. Inset show the distribution in z, and the dispersion effect caused by the flow profile.

Trajectories and theoretical predictions of particle concentration profiles in parallel plate geometries has been studied in [16, 54].

2.7 Summary

In this chapter we have advanced the understanding of microchannel acoustophoresis by exploring a number of important phenomena that affect the motion of a particle. The acoustic radiation force stem from scattering of an sound wave, incident on the particle. The force on a particle varies sinusoidally over the width of the channel and through careful choice of actuation frequency the effect of longitudinal modes can be expected to be minimal in this long geometry. Moreover, the sign and magnitude of the force depend on the density and compressibility of the particle relative to the suspending fluid.

Two phenomena that may be cause for some concern are both related to the motion of the suspending fluid. One is the acoustic streaming that induce rotation of the fluid. The second is the effect of the Poiseuille flow profile that impose a strong z-dependency on the trajectories of particles. Interestingly, both phenomena become more pronounced for flat geometries where the sound propagates along the width dimension. In the coming chapter, that covers the separation of cells and bio-affinity microbeads in such systems, these two effects are the main concerns regarding performance.

3

Separation

This chapter treats two different types of acoustophoretic operations related to separation. First, a so called medium exchange, or washing, where particles or cells are transferred from one suspending fluid into another. The second is the separation of cells or objects in similar size range based on intrinsic physical properties.

The H-separator

Originally the concept of particle separation in continuous flow by means of a transverse forces stems from Calvin Giddings. In its first embodiment, a gravitational force field was used to separate microbeads of different sizes [55]. The name H-separator reflects the layout, in which two fluids are aligned and introduced to a main channel from two opposing side inlets. At the end of the channel the flow is split up in two fractions again. During the passage through the main channel, species is selectively transferred transversely to the flow by means of some force potential, **Fig. 3.1(a)**.

Johnson and Feke was first to implement this separation strategy for acoustic half wavelength resonators [56]. In 2004 Hawkes presented a microscale half wavelength H-separator for continuous cell washing and mixing [32], it was demonstrated on a model sample of yeast cells and fluorescein dye, **Fig. 3.1(b)**.
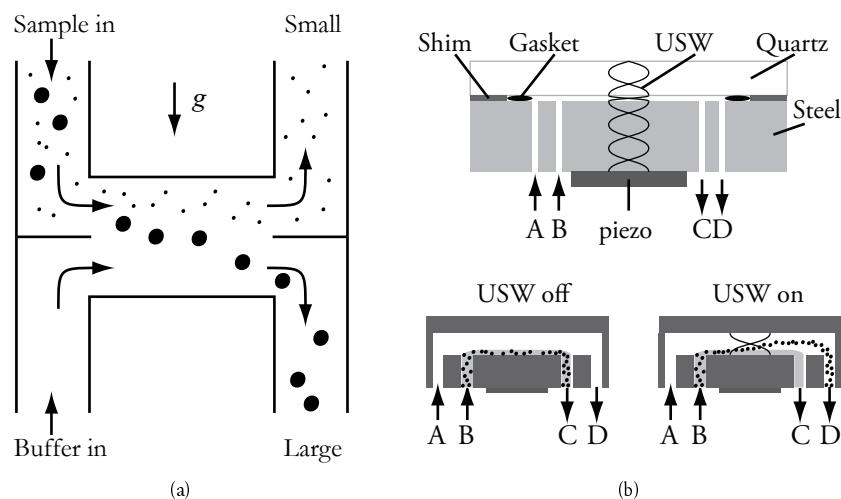
Figure 3.1: (a) The H-separator first presented by Calvin Giddings and (b) the half wavelength H-separator for continuous cell washing and mixing [32].

The 2Y-separator

A nifty configuration for acoustophoresis buffer exchange in half wavelength resonators is the so called 2Y-separator (double Y) shown in **Fig. 3.2(a)**. (A more illustrative short hand notation would rather be, a 2ψ-separator). This design was introduced and thoroughly characterized in a publication by Petersson *et al.* [24]. A similar design was later used for size discrimination of microbeads and blood cells, the main difference being that the number of outlet branches was increased [25]. A particle suspension is introduced along the side walls of an acoustophoresis channel while the exchange/wash buffer is infused in a central inlet. As the particles flow along the channel, the acoustic radiation force potential will drive them towards the centre of the channel, into the central stream of exchange buffer. At the end of the channel, the flow is split into a central outlet for the particles in new buffer, and two side outlets containing the original buffer and any particles of low acoustophoretic mobility. The symmetric layout of the inlets and outlets is well suited for half wavelength resonators that have a central acoustic pressure node.
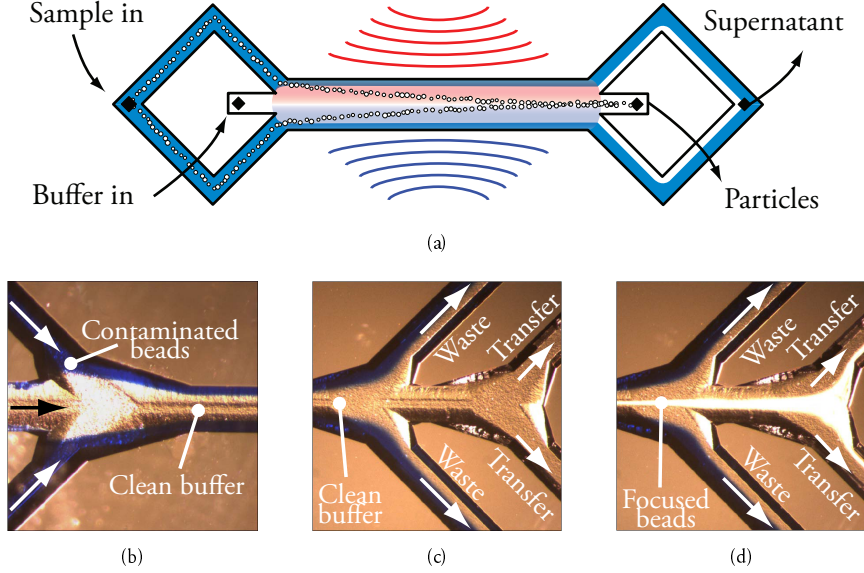
Figure 3.2: (a) A schematic of the buffer exchange principle introduced in [24]. Particles (white) in contaminated carrier fluid (blue) are introduced through a common side's inlet. Particles are drawn to the centre of the channel by the acoustophoretic force potential while the blue fluid remain unaffected at the sides. Experimental images of (b) the inlet of the channel, the trifurcation outlet (c) before onset of ultrasound, and (d) during ultrasound actuation.

3.1   Particle – medium separation

In this section, some of the fundamental transport phenomena in microchannel acoustophoresis are discussed. The fundamental operation is to transfer particles or cells from their initial suspending fluid near the walls to a new carrier fluid occupying the central part of the channel. The main focus will be to evaluate all phenomena by which minute species, much smaller than the particles, can be transported to the central outlet. In other words, we will try to understand how to avoid poor separation results. **Fig. 3.3** introduces the setting. We recall that x, y, and z denote position along the length, width, and height, respectively.

To separate particles, or cells, from minute species, the volume flow rates in the inlets and outlets

$$Q_{\text{tot}} = Q_{\text{sample}} + Q_{\text{wash}} = Q_{\text{aperture}} + Q_{\text{waste}} \tag{3.1}$$

and the acoustic energy density E_{ac} are adjusted so that the particles reach the channel centre just before arriving at the outlet trifurcation. Since according to (2.13a), the transverse velocity u_{rad} of a particle is proportional to the square of its radius a, any species of radius $<< a$ will be efficiently filtered away, regardless of their acoustic properties.

Figure 3.3: Schematic of acoustophoresis carrier medium exchange. Q denotes volume flow rate in the inlets and outlets.

By adjusting the relative flow rates to the inlets, Q_{sample} and Q_{wash}, and the outlets, Q_{aperture} and Q_{waste}, it is possible to tune the distance $w_{\text{clearance}}$ th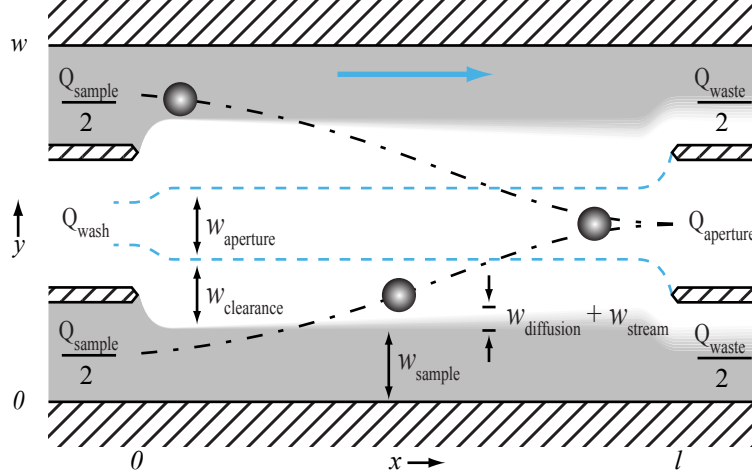at a particle must travel on order to reach the central outlet. To maximize $w_{\text{clearance}}$ the central buffer flow Q_{wash} can be increased relative to Q_{sample} while minimizing the central outlet flow rate Q_{aperture}. The selectivity and stability of the system can be expected to depend strongly on $w_{\text{clearance}}$. Such a clearance will only exist under the condition $Q_{\text{wash}}/Q_{\text{sample}} > Q_{\text{aperture}}/Q_{\text{waste}}$. To avoid diluting the central outlet fraction, one can set $Q_{\text{sample}} = Q_{\text{aperture}}$. For this configuration, transfer of particles occurs (to some degree of approximation) symmetrically over the regions of highest acoustophoretic velocity ($y = w/4$ and $y = 3w/4$), which is also favourable in terms of energy efficiency.

Some level of contamination in the central outlet is of course inevitable and can be attributed to any or one of the following sources: Diffusion of the contaminant, acoustically induced streaming in the lateral cross-section of the flow, non-specific binding of the contaminant to the particles, hydrodynamic interactions between particle and fluid, and perturbations in the flow induced by either bubble formation or oscillations in the external fluidics.

To gain understanding of the transport of contaminant from the sample inlet to the central outlet, each contribution will be discussed and estimated. To strengthen the arguments, results from paper II, Ref. [24], and Ref. [32] are referenced. Some of the effects are related to the acoustic energy density E_{ac}. Implicitly those effects are related to the bead size since a certain acoustic energy density is required to transfer beads from the side of a channel to the central outlet, for a specific flow configuration. Some bold approximations will be necessary in the following. One of these is that a particle's average velocity $\langle u_y \rangle_y$ across the channel is related to the average flow velocity in the channel

through

$$\frac{\langle u_y \rangle_y}{w/2} \approx \frac{Q_{\text{tot}}}{Lwh} \Rightarrow \langle u_y \rangle_y = \approx \frac{Q_{\text{tot}}}{2Lh}. \tag{3.2}$$

This describes the trajectory of a particle for a constant force in the y-direction and a plug flow along the channel. The beautifully curved particle trajectories derived in chapter 2 are now reduced to a straight line.

Diffusion

Diffusion of a contaminant from the side inlet to the central outlet can be investigated by comparing the time scale for one passage in the device $\tau_{\text{pass}} \approx Lwh/Q_{\text{tot}}$, to the typical diffusion time τ_{diff} over the distance $w_{\text{clearance}}$. For the smallest molecules the diffusion constant D is in the order of 10^{-10} m/s. To avoid any notable influence of diffusion, the passage time in the device should be set to less than a second, for $w_{\text{clearance}} = 100$ μm. The broadening w_{diff} of the sample stream can be expressed

$$w_{\text{diff}} \approx \sqrt{D\tau_{\text{pass}}} = \sqrt{D\frac{Lwh}{Q_{\text{tot}}}}. \tag{3.3}$$

This indicates that to minimize diffusion, the flow velocity in the device should be high. This can be achieved either by increasing the volume flow rate Q_{tot}, or by reducing the channel dimensions.

In Ref. [32] is reported that for the system shown in **Fig. 3.1** diffusion effects are significant for fluorescein molecules ($D \approx 5 \times 10^{-10}$ m/s). It was suggested that by increasing $w_{\text{clearance}}$ the contamination due to diffusion could be reduced.

Acoustic streaming

From section 2.4 we know that acoustic streaming convect fluid in the transverse cross section of the channel. At $z = 0$ and $z = h$ the streaming is directed opposite to the motion of the particles and can therefore not transfer any contaminant to the central outlet. For $z = h/2$, however, the streaming u_{str} coincides with the acoustophoretic velocity of particles u_{rad}. During one passage time τ_{pass} the broadening w_{str} due to streaming can be expressed

$$w_{\text{str}} = u_{\text{str}}\tau_{\text{pass}} = u_{\text{str}}\frac{w/2}{u_{\text{str}} + u_{\text{rad}}} \approx \frac{w/2}{1 + \frac{4\Phi\rho_o c_o a^2 k_y}{9\eta}} \tag{3.4}$$

where τ_{pass} expressed in terms of the time it takes for a particle to traverse $w/2$ under the influence of the acoustic radiation force (**Eq. 2.13a**) and acoustic streaming (**Eq. 2.14**).

Ref. [24] reports that, polyamide microparticles were washed from a dye in a configuration where the system was initially tuned so that particles were focused precisely before the end of the channel. The acoustic energy was thereafter increased 5-fold ($E_{\text{ac}} \propto$

U^2_{piezo}), resulting in a dramatic increase in contaminant transfer. **Eq. 2.15** state the ratio $u_{\text{str}}/u_{\text{rad}} \approx 0.20$ for the particle type in the experiment. This suggests that the streaming velocity, in the case of the 5-fold acoustic energy, was of the same magnitude as the acoustophoretic bead motion for the first setting. Similarly, in Ref. [32] yeast cells are reported to reach their intended outlet at 25% of the enery level required to induce significant amount of acoustic streaming. In conclusion, the acoustic energy should be tuned so as to precisely focus particles to the central outlet.

Non-specific binding

In the sample inlet, each bead is associated with an average number of non-specific contaminant molecules. The total number of molecules that can potentially be transferred to the central outlet, through non-specific binding is therefore proportional to the concentration of beads in the suspension. In paper II, particle concentrations were evaluated in the range 5×10^6 mL to 10^9 mL. In that range, the contamination per bead was indeed found to be constant, which is a rather trivial result.

It can be speculated to what extent molecules have time to come loose from the surface of a microbead during the passage of $w_{\text{clearance}}$. The number of molecules bound to a surface at a specific time point is related to the concentration of molecules in the fluid and the affinity constant $K_{\text{a}} = \frac{\text{on-rate}}{\text{off-rate}}$, which relates the probability for a molecule to stick on the surface to the probability of a molecule coming loose. When the surrounding fluid is exchanged, the system is out of equilibrium and molecules of high off rate will be depleted on the surface. This effect is however not easily detected since equilibrium will be reached in the outlet sample containers.

Hydrodynamic interactions between particle and fluid

When a sphere is dragged through a fluid by some force F_{rad}, it will exert that same force on the fluid through friction at the surface (**Eq. 2.12**). **Fig. 3.4** illustrates how the concentration profile of a contaminant in the interface between two fluids is affected by a sphere passing through the interface. The particle cause a local perturbation in the velocity of the fluid and thereby drags convects contaminant along its trajectory. At a distance of approximately 10 particle diameters from the interface the concentration of contaminant close to the surface of the sphere is greatly reduced. Clearly, as the number of particles increases in a suspension, the combined volume force exerted on the fluid increases linearly. This volume force cause convection of the fluid, and when this velocity becomes substantial relative to the velocity of the individual beads, the beads can be considered to be hydrodynamically coupled. Such hydrodynamic coupling has been studied in a paper by Mikkelsen *et al.* [57]. Numerical calculations for 1 μm paramagnetic beads in a magnetic field yielded that the hydrodynamic interaction between spheres is minimal for concentrations up to 10^8 mL which correspond to an average inter particle distance $d \approx 20$ μm. For higher concentrations the interaction increases exponentially, and at 10^{10} mL ($d \approx 5$ μm) the particles are fully coupled and thus drag along all intermediate fluid. In paper II the effect of increasing particle concentrations was investigated. In

retrospect, the range of particle concentrations was too small to reveal the hydrodynamic break down. Petersson *et al.* carried out a similar experiment in the range 5×10^{10} mL to 2×10^{11} mL, using polyamide beads ($a = 2.5$ μm). From that experiment it is clear that the washing efficiency decreased dramatically for concentrations above 10^{11} mL. Ref. [32] reports a breakdown at a concentration of yeast cells of 10^8 mL which is considerably lower. It is reasonable to assume that this break down was caused by hydrodynamic coupling between particles.
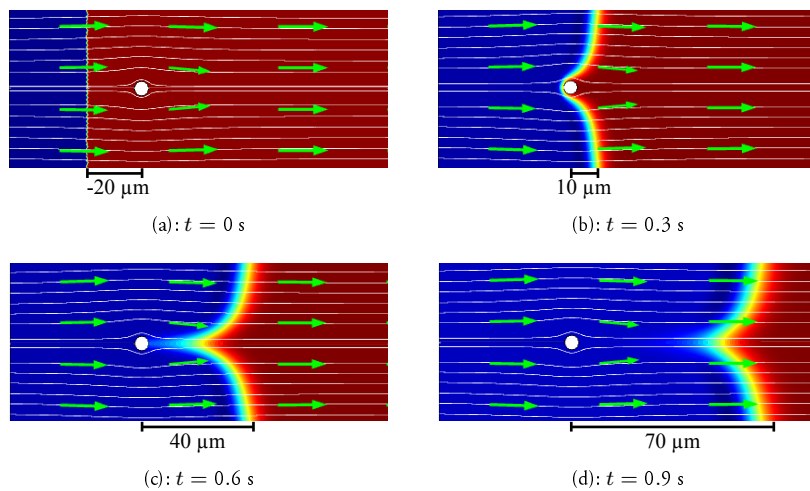
Figure 3.4: A Comsol simulation of a sphere moving through an interface between two fluids. The concentration profile of the contaminant (red → high, blue → low) is clearly affected by the drag from the sphere. Rather than moving the sphere, the suspending fluid was modeled to move at constant velocity.($a = 2.5$ μm, $u_{\mathrm{rad}} = 100$μm/s and $D = 10^{-11}$ m^2/s)

Flow perturbations

Reproducibility and efficiency of the system rely on stable flow conditions. Consider a situation where the flow in the channel is temporarily disrupted by a short plug of air entering the channel inlet and passing through main channel, causing complete mixing of the two inlet streams. Before and after this disruption the separation is ideal, i.e. no contaminant is transferred to the central outlet. The impact of such a perturbation can be estimated from the channel dimensions, and the flow rates in the inlets and outlets. The number of molecules in the channel at complete mixing can be expressed as

$$N_{\mathrm{channel}} = \frac{C_{\mathrm{sample}} V_{\mathrm{channel}} Q_{\mathrm{sample}}}{Q_{\mathrm{tot}}}. \tag{3.5}$$

27

The central outlet concentration will be the fraction of those molecules that reach the central outlet sample divided by the final volume of the processed sample.

$$C_{\text{outlet}} = \frac{N_{\text{channel}} Q_{\text{aperture}}}{Q_{\text{tot}} V_{\text{outlet}}} \tag{3.6}$$

Inserting some relevant numbers for a separation setup and a processed volume of 1 mL, yields a contamination level of 10 ppm in the central outlet fraction. Papers I and II deals with washing of molecular species from microbeads. In the context of bacteriophage antibody library selections, it can be noted that this level of contamination corresponds to a two times repeated manual washing procedure. This type of disturbances to the flow is one of the main concerns regarding stability and reproducibility in microfluidic cell handling systems in general.

3.2 Separation of cells based on acoustophysical properties

This section deals with the transport of cells in microchannel acoustophoresis. From section 2.6 it is clear that the trajectory of a particle is an intricate function of the acoustic field through the radiation force potential and the acoustic streaming, and the Poiseuille flow profile. Importantly, the particles initial position (y_{p}^{in}, z_{p}^{in}) in the transverse cross section has a major impact on the trajectory. At the end of the channel, the particles position $y_{\text{p}}^{\text{out}}$ and the outlet flow configuration ($Q_{\text{aperture}}/Q_{\text{tot}}$) determine through which outlet the particle exit the channel. The parameters contributing to $y_{\text{p}}^{\text{out}}$ are:

Particle: size a^2, mass density ρ_{p}, and compressibility κ_{p}

Fluid: viscosity η, mass density ρ_{o}, and compressibility κ_{o}

Flow field: flow rate Q_{tot}, channel geometry (L, w, h), and the particles initial position (y_{p}^{in}, z_{p}^{in})

Acoustic field: pressure field $p(x, y, z)$ and velocity field $\boldsymbol{v}(x, y, z)$

A cell of a certain species has three intrinsic acoustofluidic properties (the shape could be a fourth property) related to its phenotype. To direct the motion of the cell, all the remaining parameters are at hand. The carrier fluid can be altered, flow rate can be tuned, the acoustic field can be adjusted and so forth. Two individual cells of different types can be separated if one ore more of their intrinsic acoustofluidic properties differ. In practice however, the situation is more complicated.

Firstly, within each species, each property can be expected to have a distribution, e.g. size variations are large in most cell populations. There is an obvious chance that two individual cells of different types have overlapping properties.

Secondly, even if two individual cells do have different properties, their acoustophoretic velocity can still be identical for a given suspending fluid. The condition for separability in a plane standing wave field can be summarized as $0 < |a_2^2 \Phi_2 - a_1^2 \Phi_1|$, where

Φ is the acoustophoretic contrast factor for a cell relative to the suspending fluid. Clearly the condition can be violated for many different combinations of properties.

In general, a perfect separation of two cell populations can not be anticipated even if their average acoustofluidic properties are different. On the positive side, there are countless conditions where subsets of a population can be isolated by tuning the properties of the suspending fluid.

To achieve a separation that is deterministic in the sense that it truly reflects the intrinsic properties of the cells, the effect of the microchannel flow profile and the random spatial distribution of cells in the inlets to the channel must be eliminated. **Fig. 3.5** shows simulated trajectories for identical particles initially at $y_p^{in} = a$ and $y_p^{in} = w - a$ and distributed along z. Clearly, particles near the top and bottom of the channel exit the channel closer to the vertical centre of the channel than do particles traversing the channel near $z = h/2$. The explanation for this is that the parabolic nature of the flow profile cause particles to flow at a lower velocity near the boundaries of the channel and they are therefore exposed to the acoustic potential during a longer period of time.
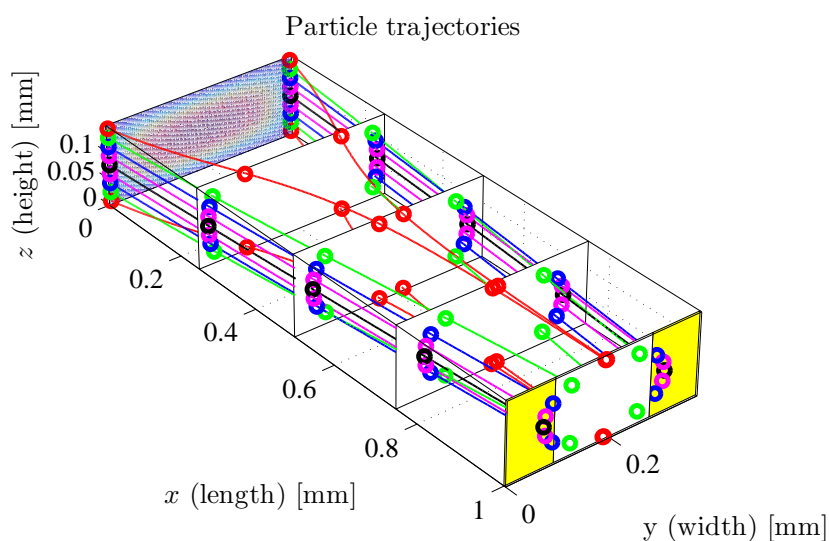
Figure 3.5: Trajectories of identical particles distributed along z and initially at $y_p^{in} = a$ or $y_p^{in} = w - a$.

From a separation perspective, this is bad news. The initial positioning of cells in the side inlet, which is typically random, results in a dramatic dispersion due to the Poiseuille flow. If not even identical particles are translated the same distance along the channel width, there is little chance that deterministic separation of cells having different properties can be achieved, given the current configuration with a trifurcation outlet. It

is not completely hopeless though, since the flow is slow near boundaries, the major part of all collected cells will have passed through regions of high flow rate where there are less of a gradient.

To eliminate the effect of the flow profile, at least three options are at hand. Firstly, the acoustic properties of the suspending fluid can be tuned so that ($\Phi_1 < 0 < \Phi_2$). Secondly, the initial positioning of the cells can be controlled. Thirdly, samples can be run repeatedly through the system until the separation become deterministic. Only the first two methods will be further discussed in the following since option number three can be expected to be associated with significant particle losses and complicated external fluidics.

Altering the acoustic properties of the suspending fluid

From **Eq. 2.11a** and **Eq. 2.11b** it is clear that two fundamental modes of separation exist. The first is when both species move in the same direction in the acoustic field, i.e. when $0 < \Phi_1 < \Phi_2$ or $0 > \Phi_1 > \Phi_2$. A second is when the particles move in opposite directions, i.e. when $\Phi_1 < 0 < \Phi_2$. In terms of stability, the latter of the two is to prefer since cells will migrate towards different spatial locations due to the opposite sign in acoustic radiation force.

In a seminal paper by Petersson *et al.* [23] it was demonstrated that lipid particles could be separated from erythrocytes, **Fig. 3.6**. In an acoustophoresis channel, half a wavelength across, erythrocytes were focused to a central vertical acoustic pressure nodal plane, while fat particles were moved towards the pressure anti-nodes at the channel walls.
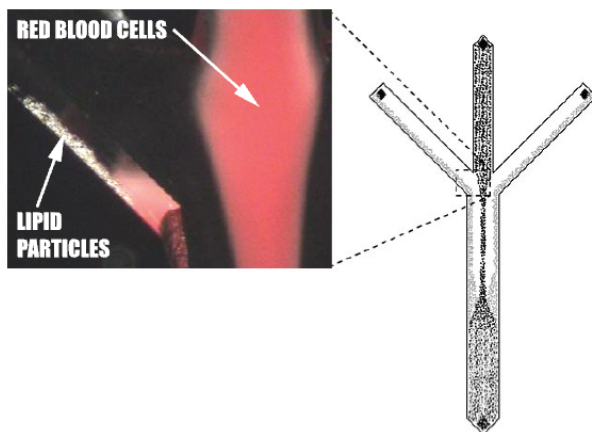

Figure 3.6: Red blood cells and lipid particles separating in an acoustophoresis micro-channel. From [58] – Reproduced by permission of The Royal Society of Chemistry.

For cells suspended in PBS, NaCl (9 g/L) or culture medium, the acoustic contrast factor (Φ) is positive. This is not surprising given that the cell is composed of a number

of solid entities each of a density higher than that of water. Similarly, the compressibility of these entities can be assumed to be less than that of water. The remaining part of the cell is water, and thus, the acoustic contrast factor must be positive.

In Ref. [25], Petersson *et al.* demonstrated how the acoustic properties of the suspending fluid can be altered to separate microbeads of the same size but of different material properties. In a first experiment the beads were found not to be separable since the relative difference in acoustophoretic velocity u_{rad} was too small. By addition of salt (CsCl) to the suspending fluid the acoustic contrast factors Φ_1 and Φ_2 of the two bead types was lowered, thereby increasing the relative difference in acoustophoretic velocity (since $u_{\mathrm{rad}} \propto \Phi$), enabling separation of the two bead types.

For cells, which have a substantially lower acoustic contrast factor than polymer beads, buffer conditions can be chosen so as to change the sign of the contrast factor. This implies that in theory it is possible to achieve binary separation between cells of different types by a change of sign in the contrast factor for one of the cells. One potential hurdle in this approach is associated with acoustic streaming and the critical radius a_{c} introduced in section 2.4. For small Φ, streaming becomes increasingly dominant. From **Eq. 2.15** a critical contrast factor Φ_{c} can be derived.

$$|\Phi_{\mathrm{c}}| = \frac{9\eta}{8\pi a^2 \rho_{\mathrm{o}} f} \tag{3.7}$$

If $\Phi < |\Phi_{\mathrm{c}}|$ for both cell types, separation is not possible. Notably, the viscosity of the fluid impact the separability condition which may impose a problem when choosing appropriate media for alteration of properties. Gradient density media such as Percoll and Ficoll that may be considered, cause a dramatic increase in viscosity at high concentrations.

No thorough study have yet been carried out to map the acoustic properties of cells and particles. Attempts have been made by the author *et al.* [59, 60] and others [61–63].

A problem inherent in having a force field directed towards a wall is the fact that particles may eventually clog the channel. This is again an adverse effect of the parabolic nature of the flow profile. When particles reach a wall, the force normal to the wall generate a friction force opposite to the direction of the flow. Since the flow rate near the wall is minimal the particle often stick to the wall. Once particles start to attach to a wall the channel gets quickly clogged. Clogging can be avoided by minimizing the acoustic energy. Lowering the acoustic energy might, however, affect the separation outcome since the species intended for the central outlet might not have time to focus. A straight forward way out of this problem would be to simply extend the length of the channel, whereby the friction force at the wall can be minimal while minute species still have sufficient time to focus in the channel.

Another approach is to make sure that particles can not reach the walls of the channel. By increasing the width of the channel from $w = \lambda/2$ to $w = \lambda$ a pressure anti-node appear in the center of the channel and two pressure nodes will be present at $y = w/4$ and $y = 3w/4$. By introducing sample in a central inlet, hydrodynamically focused by carrier fluid from each side, particles of positive Φ-factor can be actively transported
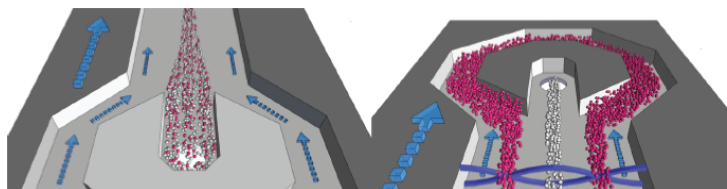
Figure 3.7: Schematic of the milk preconditioning device presented by Grenvall *et al.* showing (left) the central inlet containing particles of opposite sign Φ-factor, and (right) the outlet where negative Φ particles (white) are maintained in the central region of the flow, while positive Φ particles (red) are moved to the pressure nodes on each side. Reprinted with permission from [64]. Copyright 2009 American Chemical Society.

away from the central stream and collected in the side outlets. Particles of negative Φ-factor will remain in the central part of the flow, where the flow rate is higher and exit through a central outlet. The hydrodynamic flow focusing prevent particles of negative Φ-factor from reaching the walls of the channel. This configuration has been presented by Grenvall *et al.* [64] for preconditioning of milk samples for quality analysis in dairy industry, **Fig. 3.7**.

Two-dimensional acoustophoresis pre-alignment

Acoustic pre-alignment of cells or particles can be employed to eliminate the dispersion effect due to the Poiseuille flow profile. To achieve this, a cell pre-alignment channel can be integrated in the chip, of dimensions chosen so that a resonance condition is fulfilled in both width and height, respectively. The chip can be actuated either using separate frequencies for each dimension or a single frequency matching both dimensions.

A capillary for two-dimensional alignment of particles in a circular geometry was presented by Goddard *et al.* in 2005 [65]. This was later demonstrated for pre-concentration and increased resolution in flow cytometry [66]. Grenvall *et al.* presented a fluorescence activated acoustophoresis sorting device in which particles were first pre-aligned to a single point in the transverse cross-section of the flow prior to detection and conditional onset of sound in a second separation channel [67]. Also, acoustic pre-alignment has been used to enhance separation in a model system of microbeads of three different sizes [68].

It is not obvious that the above mentioned single frequency actuation can lead to acoustophoretic motion along two directions simultaneously. **Fig. 3.8(a)** and **(b)** show the resonant modes in the yz-plane for a channel of $w = 2h$ actuated at $f = c/\lambda = c/w = 5$ MHz.

The two eigenmodes can exist simultaneously in the same cross section even though the frequency is the same. In experimental practice, particle motion in y and z, of same order of magnitude, is evident for this somewhat naive extrapolation from one to two dimensions. At the end of such a channel, the particles are focused vertically and divided into two streams horizontally, i.e. positioned at coordinates $(l, w/4, h/2)$ and

$(l, 3w/4, h/2)$. The phenomenon has not yet been characterized in depth regarding the transient motion of particles and no hypothesis will be presented here but acoustic energy is apparently distributed evenly between the modes. The peak width of acoustophoresis resonant modes has been studied in Ref. [48].

Resonance patterns in two dimensions can also be found for higher frequencies. **Fig. 3.8(c)** shows a mode which is in agreement with **Eq. 2.4** $f = \frac{c}{2}\sqrt{4/w^2 + 1/h^2} \approx 7\,\mathrm{MHz}$. This mode can however not be expected to transport particles as efficiently to two points in the cross section, rather particles would be collected in the nodal grid $y = w/4, y = 3w/4$ and $z = h/2$.
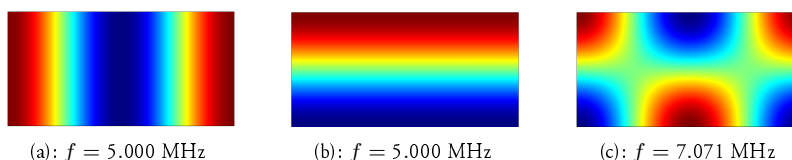

(a): $f = 5.000$ MHz   (b): $f = 5.000$ MHz   (c): $f = 7.071$ MHz

Figure 3.8: Resonant acoustic pressure field in the transverse cross section of an acoustophoresis channel of width ($w = 300\ \mu m$) and height ($h = 150\ \mu m$). In a fluid surrounded by hard walls, $c_o = 1500$ m s^{-1} and $\rho_o = 1000$ m^3 s^{-1}

In paper V, an acoustophoresis pre-alignment channel was integrated with an acoustophoresis separation chip to achieve high resolution cell separation of circulating tumour cells from blood cells, **Fig. 3.9**. In a cell pre-alignment channel (2), the width ($w_1 = 300\ \mu m$) and height ($h = 150\ \mu m$) were chosen so that ultrasonic vibrations ($f_1 = 5$ MHz) generate two acoustic pressure nodes along the channel width and an additional single acoustic pressure node along the channel height (insets). The acoustic force potential deflects the motion of cells flowing through the channel so that, near the end of the channel, cells are confined to two parallel bands, oriented along the flow, and elevated at distance $h/2$ above the channel floor. The two bands are bifurcated (3) to both sides of a central buffer inlet (4) and enter a second channel laminated near the walls.

In the cell separation channel (5), the width ($w_2 = 375\ \mu m$) is matched to a second ultrasound frequency ($f_2 = 2$ MHz) to generate a single acoustic pressure node in the vertical centre of the channel. The acoustic force on the pre-aligned cells direct their motion towards the central node at a rate determined by the cell size, the density, and compressibility.

Paper V reports a dramatic improvement in resolution when acoustophoresis pre-alignment is activated as compared to when the pre-alignment is off. This was demonstrated by separation of polystyrene beads of diameters 5 μm and 7 μm.

In an ideal case, the separation in the device is deterministic and will perfectly reflect the intrinsic properties of the cells or microbeads. Assuming a sample of particles of uniform size and material, for a given flow rate, all particles would exit the channel either through the side's outlet, or through the central outlet, solely depending on the applied acoustic energy density E_{ac}. Moreover, the transition from common side's outlet to centre would be instant, as plotted in **Fig. 3.10**. All deviations in acoustofluidic prop-
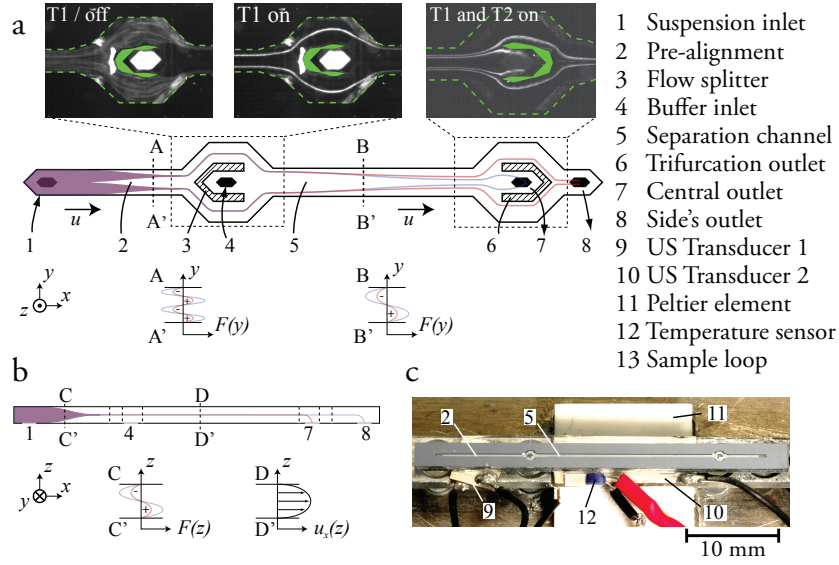
Figure 3.9: Acoustophoresis microfluidic chip for pre-alignment and subsequent separation of cells or microbeads. (a) Top view schematic of the channel, and (b) side view schematic. (c) Photo of the device.

erties or imperfections in flow etc. will inevitably impose a less sharp transition. If, to a first approximation, all deviations in particle trajectories are assumed to have a normal distribution, the relative amount of beads in the central outlet Y_{centre} can be described by a so called cumulative distribution function (3.8). **Fig. 3.10** shows a plot of Y_{centre} as function of acoustic energy density E_{ac} for a transition energy E_{tr} of $0.5\,\text{J/m}^3$ (arbitrary scale).

$$Y_{\text{centre}} = \frac{1}{2}\left[1 + \text{erf}\left(\frac{E_{\text{ac}} - E_{\text{tr}}}{\sigma\sqrt{2}}\right)\right] \tag{3.8}$$

In Paper V (**Fig. 2**), Y_{center} was fitted to experimental data for bead samples of diameters 5 µm and 7 µm, using E_{tr} and σ as fitting parameters. From simulations of particle trajectories for the flow configuration in the experiments, a theoretical t'transition energy $E_{\text{tr}}^{\text{teor}}$ could be estimated. This method was used to calibrate the separation system before each cell separation experiment, i.e. to find appropriate piezo actuator voltages. An extension of this analysis could be to assess system performance by more carefully studying the slope of the transition, σ. E.g. by incorporating a measured distribution of bead sizes into the model.

As most often, there is a downside to this acoustic pre-alignment strategy. For in-
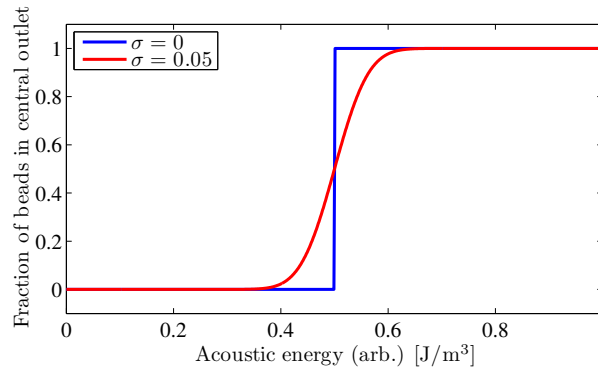
Figure 3.10: Plot of the relative amount of beads in the central outlet for increasing acoustic energy E_{ac} and a transition energy $E_{tr} = 0.5$ J/m^3, **Eq. 3.8.** For perfectly aligned and identical particles the transition is sharp (blue line). All imperfections in the system introduces a distribution σ which makes the transition smoother.

creasing cell concentrations, separation will inevitably break down due to hydrodynamic interactions, see section 3.1. Due to the confinement of particles in the transverse cross section there is an evident risk that the capacity of the system, in terms of cell concentration, becomes dramatically reduced. Also, until this effect has been more thoroughly investigated, above experiments and simulations of particle trajectories, cannot be used for absolute measurements of the acoustic energy density in the channel due to a potentially reduced Stokes drag on the particles. For the purpose of system calibration, however, the method is valid as long as the concentration of calibration beads is kept constant.

3.3   Summary

This chapter may have given the reader some insights to the complexity of microchannel acoustophoresis separation systems. First the basic operating configurations of microchannel acoustophoresis separation devices was presented. Thereafter merits and limitations was discussed for applications involving medium exchange of particles in suspension. Results reported in paper II, Refs. [24], and [32] was recalled to establish relevance for some of the phenomena. Diffusion effects can be avoided by increasing the flow velocity and or by increasing the travel distance for a particle in the transverse direction. Lateral acoustic streaming must be considered to be significant for small particles, and care must be taken not to run systems at higher energy levels than necessary. Hydrodynamic interaction between particles was argued to be detrimental for separation of particle rich suspensions.

On the subject of cell separation, it was concluded that a minimal requirement for perfect separation for cells of different types is to have a deterministic separation mecha-

nism, meaning that all identical cells must be separated to the same outlet. One strategy for achieving this is to choose a carrier fluid in which the cell types have opposite sign in acoustic contrast Φ. Another strategy was that reported in paper V where cells are acoustically pre-aligned prior to separation to eliminate dispersion due to the Poiseuille flow velocity profile.

4

Measuring the acoustophoretic velocity field

In macroscopic systems, an acoustic field can be directly characterized using a hydrophone. Inside a microchannel, hydrophone measurements is obviously not a viable route due to the restricted geometry. Actually, any type of measurement probe inserted into the channel is likely to interfere with the resonance in the channel. To impose minimal perturbation of the system it has throughout the history of the research-field been customary to study the motion of small spheres (i.e. $a << \lambda$) suspended in the acoustic field. Kuntd measured the speed of sound in fluids by studying nodal positions of dust particles [2], Klein measured sound intensity indirectly by recording the deflection of a metal sphere suspended in a torsion pendulum, and Mandralis and Feke calibrated the acoustic field in a separation channel by levitation of particles [16]. Hagsäter *et al.* was first to measure the acoustic resonant modes in an acoustophoresis microchannel in two dimensions by micro particle image velocimetry (PIV) [69], and Barnkob *et al.* studied the the pressure amplitude frequency dependency in such channels by measurement of particle trajectories [48].

In microsystems, where viscous forces dominate over inertial forces, a velocity measurement of a spherical particle can be directly translated to a force through $\boldsymbol{F}_{\mathrm{rad}} = \boldsymbol{F}_{\mathrm{d}}$, see **Eq. 2.12**. From (2.9) it can be deduced, that for an arbitrary acoustic field, measurement of the acoustophoresis force field $\boldsymbol{F}_{\mathrm{rad}}(x, y, z)$ can not be used to fully determine the acoustic velocity field $\boldsymbol{v}_1(x, y, z)$ and the pressure field $p_1(x, y, z)$. If, however, the acoustic pressure field can be described by a cosine product, as hypothesized in **Eq. 2.3** (**Fig. 2.2**), then $\boldsymbol{v}_1$ and p_1 are related through **Eq. 2.5**, whereby measurement of $\boldsymbol{F}_{\mathrm{rad}}$ fully determines the acoustic field.

To test the presented theoretical model of chapter 2 experimentally, a rather extensive study was carried out which is reported in greater detail in paper VI. To measure the acoustophoretic velocity field of microbeads, the method proposed by Hagsäter *et al.* [69], micro PIV, was implemented. The main scope was on assessment of system stability, temperature and frequency dependency and the spatial variation of the velocity field along the length of the channel.

4.1 Measurement system

A schematic of the system is shown in **Fig. 4.1** and a photograph is shown in **Fig. 4.2(a)**. Briefly, particles were infused in the channel from a syringe pump and the flow was temporarily stopped. A high speed camera was triggered at the onset of ultrasound in the system and the first couple of frames was stored, capturing the initial motion of microbeads. Thereafter new beads were infused and the process was repeated. Temperature was controlled to a precision of approximately 0.2 °C. Images were acquired for a range of acoustic frequencies, chip temperatures, acoustic actuator voltages. For three identified resonance frequencies, a $l = 12$ mm long section of the channel was analysed.
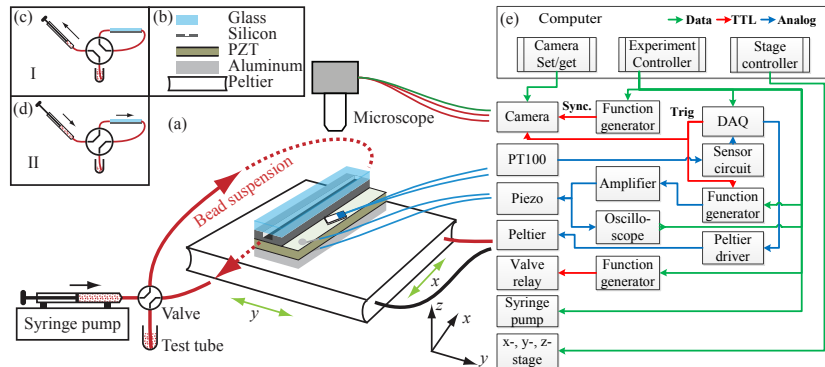
Figure 4.1: Setup for the automated system for micro-PIV measurements of acoustophoretic velocity fields. (From Augustsson *et al.*, Lab Chip, 2011)

4.2 Micro-PIV analysis

In micro-PIV [70–74], time resolved microscope images (frames) of particles are analysed through cross-correlation to determine the velocity field. The frames are subdivided into smaller units, so called interrogation areas, each of which will be associated with a velocity vector. A given interrogation window, centred around (x_n, y_m) in the first image frame, is cross correlated with the corresponding window in the second image frame. The peak in the cross-correlation function is a measure of the local displacement of the particles,

from which the particle velocity $\boldsymbol{u}$ is derived. Each particle is manifested on an image by an spatially confined intensity profile. If the combined intensity profiles of the particles from the first frame correspond perfectly to the intensity profiles of the second frame the velocity of the particles must be zero. If the particles have a velocity $\boldsymbol{u}$, the two frames must be displaced a distance $\boldsymbol{r} = \Delta t \cdot \boldsymbol{u}$ to correlate. The optimal displacement is found by calculating the sum of the products of overlapping pixel intensities for all possible displacements, and thereafter looking for a maximum in this correlation function. To achieve high quality velocity fields it is customary to repeat the measurements up to 100 times. For each interrogation window an average correlation function can be calculated, from which the velocity vector is deduced.

4.3 Measured acoustophoretic velocity fields

In brief summary the results were the following: The system is stable enough to perform repeatable data assessment for several days. It was also found that a main contributor to instability could be attributed to temperature changes. Temperature effects in acoustophoresis systems were found to be significant even for small changes in temperature. A 5 °C temperature change was demonstrated to render a $\sim$50% reduction in acoustic velocity amplitude within one field of view 850 μm. Also, the resonance frequencies in the channel was found to depend on temperature. This comes at no surprize since the speed of sound in water depends strongly on temperature and this will affect the resonance condition for the standing wave, see **Eq. 2.4**.

The characterization of the global acoustophoretic velocity field revealed that the velocity of microbeads along the width w of the channel is well described by a sine-function throughout the whole examined length in accordance to theory, section 2.2, **Fig. 4.2(b)**. Comparing the global velocity field along the length l to a theoretical velocity field in two dimensions, yield an apparent correspondence to theory, **Fig. 4.2(c)** and (**d**). From a quantitative analysis of the variation in acoustophoretic velocity magnitude along x can not be fully described by the theoretical model. Data could neither confirm, nor completely rule out the hypothesis about an acoustic pressure field of the form $p = p_{\mathrm{a}} \cos(k_x x) \cos(k_y y)$. The walls of the channel are not perfectly hard compared to the fluid as stipulated in the model. Geometry variations along the length of the channel due to fabrication imperfections may also affect the longitudinal resonances. Moreover, the piezo transducer modes and the coupling of acoustic energy to the chip presents other sources of uncertainty, not included in the model.
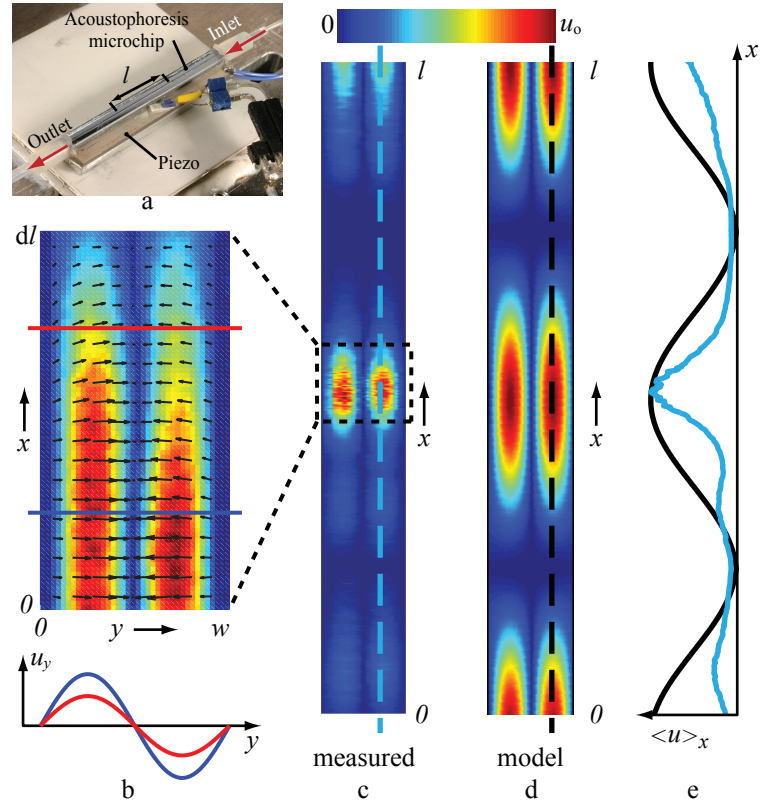
Figure 4.2: Acoustophoretic velocity field of microbeads measured by micro PIV along a $l = 12$ mm section at the center of the channel. (**a**) Photograph of the acoustophoresis microchannel. (**b**) Measured acoustophoretic velocity field for $a = 2.5$ μm polystyrene microbeads within one field of view. (**c**) Composition of the 15 adjacent measured velocity fields along l and for reference, (**d**) theoretical velocity field for polystyrene beads for an two-dimensional acoustic pressure field $p = p_a \cos(k_x x) \cos(k_y y)$. Dimensions in (**c**) and (**d**) are not to scale. Real aspect ratio is 32. (**e**) Plot of the mean acoustophoretic velocity as a function of longitudinal position, for measured (cyan) and modeled (black) data.

4.4   Summary

The acoustic resonant modes in acoustophoresis microchannels are not yet fully understood. The transverse acoustophoretic velocity field is, however, well described by a sinusoidal in accordance with theory, and the magnitude variation is relatively slow in the longitudinal direction. In a continuous flow setting, this implies that a one-dimensional acoustic pressure field is a valid approximation for calculating a particles transverse posi-

tion at the end of the acoustophoresis channel. Also, the model for acoustic streaming in section 2.4 is thereby valid. An improved theoretical model should most certainly incorporate also the surrounding chip material and the piezo transducer. Experimentally, the asymmetry in the longitudinal direction is a cause for some concern. To accommodate for such modes, a model must incorporate some sort of damping of arbitrary nature, which is clearly aggravating from an experimentalists point of view. If, in the future, conjecture between experiment and model can be demonstrated through theoretical insights and improved engineering capabilities, chances are good that microchannel acoustophoresis devices can become more stable, energy efficient and versatile in life science applications.

5

Realization of an acoustophoresis device

This chapter presents, the process of fabrication and assembly of an acoustophoresis microchannel. As an illustrative example, the device of paper V will be used, **Fig. 1.2(a)**. The acoustophoresis microchannel structure was etched in a <100> silicon wafer (76 mm × 350 μm) using so called KOH-lithography.

Producing a mask.

First, a glass/chromium mask was produced from a pattern defined in a CAD-file. A thin UV-laser spot scanned the surface of a thin film of positive photoresist deposited on the surface of the chromium, exposing only those areas defined in the CAD-file. The exposed resist was then removed by a developer so that the chromium could be etched away.

Silicon dioxide patterning.

The silicon wafer was heated to 1100 °C for 6 h, whereby a thin layer of silicon dioxide formed on the surface. Thereafter one side of the wafer was spin coated with a thin layer of positive photoresist onto which the pattern from the mask was transferred by UV lamp exposure. After developing the photoresist, the areas of uncovered silicon dioxide were etched away using buffered hydrofluoric acid. Thereafter the unexposed photoresist was removed by rinsing in acetone. The silicon dioxide works as a mask in the next step of the process.

Etching a channel.

The silicon wafer was immersed in potassium hydroxide (KOH) at 80 °C for a few hours, until a channel of desired depth has formed in the silicon. The etch rate of KOH in silicon dioxide is very slow compared to that of silicon. This, in combination with the crystalline property of the silicon, results in a rectangular cross section channel, if the channel is oriented along one of the <100>-directions.

After etching the channel, the remaining silicon dioxide was removed, the wafer was cleaned using RCA-wash and the surface was once again oxidized. The whole process was repeated to etch holes for inlets from the back side of the wafer.

Comments on channel aspect ratio.

The fact that the etch rate is uniform in the downward and the sidewards direction restricts the aspect ratio ($\frac{h}{w}$) of the channel to $< \frac{1}{2}$. In the CTC-chip, one of the segments is designed to have this maximal aspect ratio. This is, however, not practically, or even physically achievable. The opening mask would theoretically have to be infinitesimally narrow, which would not allow any diffusion of chemicals to contact with the silicon. The slight deviation from optimum aspect ratio did not display any adverse effect on the performance of the device. To produce channels of arbitrary aspect ratio one can instead use <110>-silicon and align the channel perpendicular to either one of the two available <111> zero etch rate planes. <110>-silicon was used in papers III and 4, included in this thesis. A common trade off is, however, a reduced design freedom as the two available stop etch planes are not orthogonal. E.g. it is not possible to create symmetric bifurcations or trifurcations for splitting and merging flows. Deep reactive ion etching is of course a very attractive alternative that combines high aspect ratio and flexible layout.

Anodic bonding.

The wafer was diced (40 mm x 3 mm) and a piece of borosilicate glass was anodically bonded to the silicon to seal the channel structure. Anodic bonding can be performed by sandwiching the silicon and glass and heating to 450 °C on a hot plate surface which also serve as an anode. A cathode is then brought into contact with the glass surface and a voltage is applied (order 1000V DC). The resulting electrostatic force between the two substrates pulls them together forming a bond that remain after removing the electric field and lowering the temperature. Notably, the rare circumstance that the thermal expansion coefficients of borosilicate glass and silicon are very similar, prevents chip rupture when cooling down.

Chip assembly.

To connect external tubing to the chip, pieces of silicone tubing were glued to the back side of the chip over each inlet/outlet hole. All parts of the chip assembly were thereafter glued together using ethyl-2-cyanoacrylat. The parts were, from bottom up: an

aluminium microscope mounting plate also serving as heat sink, a Peltier element for temperature control, an aluminium bar to distribute heat evenly, two piezoceramic transducers (one for each acoustophoresis channel), and finally the acoustophoresis chip. A Pt100 thermo-resistive element for temperature measurement was glued onto the PZT alongside the acoustophoresis chip.

Temperature control.

The temperature is monitored and controlled in a closed loop connected to the Peltier element. The effect of temperature fluctuations on the resonance pattern and magnitude is discussed in more detail in chapter 4. Another aspect of the temperature control is the possibility to set the temperature to either 37 °C for cell experiments or to lower the temperature to perform experiments "on ice". Moreover, lowering the on chip temperature relative to the input buffer temperature can be a way to reduce bubble formation inside the channel since the solubility of a gas increases with decreasing temperature and therefore there will be a net transport of gas molecules out from the device.

Driving a flow.

The external fluidics is important in sample preparation systems. To produce accurate and reliable flow rates, syringe pumps have been used in the work presented herein. Peristaltic pumps, pressure chambers and water columns are other ways to produce flow in a microchannel. Pressure driven systems and peristaltic pumps are advantageous in that it is possible to have more than one open end in the system. Sample can be withdrawn from one test tube and extruded into another with minimal retention time in the system. The downside of peristaltic pumps is the generation of oscillating flow. For pressure driven systems, sensitivity is high for variations in fluid resistance.

Infusion and collection of sample.

To ensure accurate volume flow rates in all parts of the channel structure, maximum one channel inlet or outlet can be open to ambient pressure. If sample is withdrawn from a test tube, the output of the device inevitable end up in the outlet syringes. In terms of sample recovery and potential for sequential processing of multiple samples this is not beneficial. To assess functionality of the separator, collection loops can be connected in series with each outlet. The loops sample the flow during a pre-determined time and are thereafter switched to extract collected samples, **Fig. 5.1**
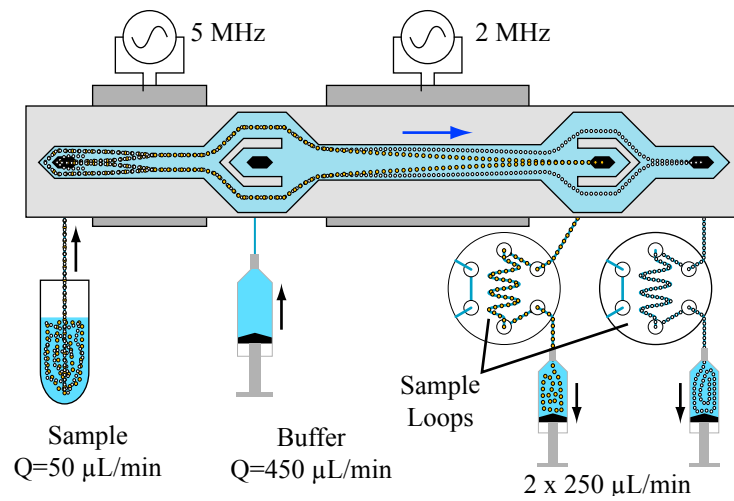
Figure 5.1: Schematic of the acoustophoresis microchannel platform for pre-alignment and subsequent separation of cancer cells (yellow) form white blood cells (white). From paper V.

6

Outlook

Interdisciplinary collaboration between physicists, engineers, biologists and clinicians is the only way to achieve clinical relevance for new methods. Nevertheless, the different frames of reference, vocabulary, and incentives, presents a big challenge in such projects. Not only must all involved researchers be highly skilled in their own field, but to this must be added, insights in other research areas. The role of the engineer in this context is most often to convert physical insights to technical reality on the one hand, and to condense knowledge about biological systems to addressable unit operations on the other.

In this thesis the focus has been highly technical. This is to some extent related to the fact that the subject contain a lot of uncovered ground. One of the most pressing tasks for the near future is therefore to demonstrate a good agreement between model and experiments. For good or bad, as long as a method it is not well described, its true potential is obscured for everyone, and it will continue to be – a promising tool for the future.

It is undoubtedly important to advance the technique by expansion to new application areas. Also, the purely technical features must progress, such as combining microchannel acoustophoresis with optical detection, incorporation of other force fields, or interfacing multiple unit operations on a single device. In contrast to this, the already established platforms must be validated and adapted to clinical reality.

In the interface between the workshop, the cell lab, and the clinic, the engineer most often discover a few things. Firstly, that many microfluidic devices are not sufficiently reliable and practical for use in a clinic. Secondly, that clinicians have very little time to spend on developing new methods. And thirdly, that there is a tendency to overrate the potential of the new technology.

The only way to get better is to practice. Likewise, the only way to bridge the gap between disciplines is to do more collaborative projects. Thereby the true potential of microchannel acoustophoresis can be unveiled.

7

Populärvetenskaplig bakgrund

Redan år 1866 publicerade den tyska fysikern August Kundt (1839-1894) ett experiment som är fundamentalt för denna avhandling [2]. Hans frågeställning var ungefär följande: Kan det vara så att små damm- eller sandpartiklar inordnar sig i ett periodiskt mönster om de befinner sig i en stående ljudvåg, t.ex. inuti en orgelpipa? Någon undrar nog, vad är en stående ljudvåg? Andra kanske undrar, vad fick han den funderingen ifrån? Någon invänder helt säkert, varför bryr han sig om vad som pågår inuti en orgelpipa, det gör väl inget om det är lite damm därinne, som inte syns? Skaffa ett riktigt jobb! Genom att besvara de två första undrandena kan jag kanske undslippa invändningen.

För att förstå vad en stående våg är så kan vi föreställa oss att vi sitter i ett badkar. Alla barn vet att om man sitter i ett badkar, så finns det mycket goda förutsättningar för att skapa en stående våg. Detta åstadkoms genom att periodiskt förflytta kroppen fram och tillbaks i badkarets längdriktning med en frekvens som exakt motsvarar vågens utbredningshastighet dividerat med badkarets dubbla längd. Mer specifikt, barnet skall avpassa sin frekvens mot den tid det tar för en våg att utbreda sig; bort från barnet till ena kortsidan, där den vänder i kaklet, tillbaks förbi barnet bort till kortsidan bakom barnet, där den vänder, och tillbaks till barnet. Precis i det ögonblicket skall en ny period påbörjas. Ganska snart kan man notera att vågorna från föregående perioder adderas till varandra, och även om det bara är ett mycket litet barn som oscillerar, så kan vågen uppnå en ansenlig amplitud.

Det finns några intressanta observationer att göra. För det första, när vågen är som högst på ena sidan av badkaret, så är den som lägst på motstående sida. För det andra, i mitten av badkaret är våghöjden noll, vi kallar det för en nod. För det tredje, i mitten av badkaret är strömningshastigheten i längdriktningen som högst. Vatten lagras upp mot ena väggen och forsar sedan tillbaks mot andra väggen. För det fjärde, om man slutar gunga så tar det ca fem cykler innan vågen dör ut. Det betyder att när den stående

vågen är i full gång så lagras varje rörelse i upp till fem cykler och summeras till en enda gemensam våg. Därför blir amplituden så hög, och därför är det viktigt att synkronisera frekvensen med längden av badkaret (kaviteten) och utbredningshastigheten. I ett mycket långt badkar så finns det möjlighet att skapa en stående våg som har flera vågtoppar på samma gång.

För att återknyta till Kundt, så byter vi nu ut vatten mot luft, badkaret byts mot en orgelpipa. Barnet byts ut mot den ljudalstrande visslan som finns längst ner på en orgelpipa. Ljudvågor från visslan fortplantar sig upp och ner genom orgelpipan, och alla frekvenser som överensstämmer med pipans längd med avseende på ljudets hastighet i luft kommer att förstärkas. Alla andra frekvenser dör ut och når aldrig våra öron.

Varför misstänkte Kundt att dammpartiklar skulle interagera med den stående vågen och ansamlas i trycknoderna? Han berättar i introduktionen av sin publikation om ett experiment utfört av en tysk/ungersk/slovakisk vetenskapsman vid namn Ernst Chladni (1756-1827) [4], men experimentet tillskrivs ursprungligen Robert Hooke (1635-1703) [75], och det går till så här.

På en tunn platta av glas eller metall strös ett tunt lager av partiklar, t.ex. saltkorn, ut. En fiolstråke anbringas mot kanten av plattan så att stående vågor uppstår vars våglängd och frekvens beror av plattans dimensioner. Amplituden är ytterst liten så det går inte se med blotta ögat, men plattans yta buktar sig upp och ner likt vattenytan i badkaret. Man kan då observera att saltkornen börjar röra på sig och organiserar sig i ett mönster som överensstämmer med noderna av den stående vågen, se **Fig. 7.1**. Förklaringen till detta är att om ett saltkorn befinner sig på en plats där det inte är en nod så kommer det att göra ett litet skutt varje gång som plattan åker uppåt. Eftersom plattan alltid buktar uppåt när kornet lämnar ytan kommer saltet hoppa lite i sidled och så småningom ansamlas i noderna. (Enda undantaget till detta är om kornet befinner sig exakt mitt emellan två noder, då är hoppet är helt vertikalt.)

Kundt visste alltså om att partiklar i vissa fall kan interagera med stående vågor. Faktum är, att vid den här tiden så hade både Félix Savart (1791-1841), Thomas Seebeck (1770-1831), och Michael Faraday (1791-1867) byggt Chladni-plattor och utforskat olika aspekter av fenomenet. Kundt insåg att det är en fundamental skillnad mellan stående ljudvågor (longitudinella) i en orgelpipa och den typ av badkarsvågor"(transversella) som man observerar på en Chladni-platta. Inne i en orgelpipa svävar dammkornet nämligen omkring, helt omsluten av den stående vågen. Om det finns en kraft som flyttar dammkornet mot närmsta nod så är det inte lika uppenbart hur det går till som i fallet med saltkornet som skuttar fram på ytan av en glasplatta.

Kundt byggde en genomskinlig orgelpipa och kunde påvisa att dammet, och ingen är nog förvånad nu, faktiskt ansamlade sig periodiskt i röret, i de punkter där man förväntar sig att hitta trycknoderna. I förlängningen kunde han använda sitt rör för att bestämma ljudhastigheten för olika gaser som han fyllde röret med genom att mäta avståndet mellan noderna. Allt sedan den dagen har experimentalister förtvivlat försökt förstå hur den här förflyttningen av partiklar faktiskt går till. Teoretiskt har man dock, ända sedan en publikation av Louise King år 1934 [7], kunnat räkna ut hur snabbt en partikel förväntas röra sig i ett sådant ljudfält.
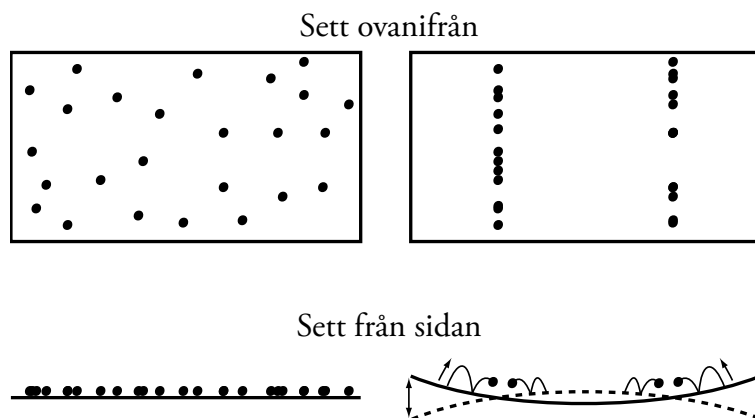
Figur 7.1: Hookes/Chladnis experiment. (Vänster) Partiklar utspridda på en tunn platta som är stilla. (Höger) Plattan sätts i svängning med t.ex. en stråke som anbringas mot kanten. Den nedre bilden visar hur partiklarna hoppar mot noderna på grund av plattans vibrationer.

Under 1990-talet utvecklades den metod som är föregångaren till den typ av system som används i denna avhandling. Det hade visat sig att det går utmärkt att skapa stående vågor i vätska och därmed flytta runt på celler eller mikroskopiska partiklar. För att kraften på partiklarna skall vara tillräckligt stark använder man sig av ultraljud i frekvensområdet 1 till 10 MHz vilket ligger långt över människans hörselomfång. Om man vill generera en stående halvvåg likt den som nämndes i exemplet med badkaret så måste man krympa dimensionen på kaviteten till storlekar mellan 0.1 och 1 mm. Ett viktigt skäl till att det dröjde ända till 1990-talet innan de första så kallade akustoforeschipen tog form hänger ihop med begränsningar i fabrikationsmetoder.

Mikroteknologin, som initialt drivits på genom utvecklingen av datorer, erbjuder just den precision som behövs för att skapa flödeskanaler av mycket små dimensioner. Detta har gett upphov till ett forskningsområde som kallas micro total analysis systems eller kort och gott, lab on a chip, **Fig. 7.2**. Här försöker man föra över moment, som normalt utförs inom kemi och biologi, till ett laboratorium i mikroskala. Några argument för att göra detta är att automatisering av processer har potential att göra dem snabbare och mer reproducerbara än manuella arbetsmoment. Ett vanligt argument är att åtgången på kemikalier blir mindre, men kanske ännu viktigare är att precision och känslighet i analyser kan förbättras avsevärt. Om man exempelvis ur 1 mL blodprov från en patient vill isolera en typ av celler som det kanske endast finns 10 st av, jämfört med alla 5 miljarder röda blodkroppar och 5 miljoner vita blodkroppar, så står man inför ett problem som är mycket svårhanterligt med traditionella labbprotokoll.

Många hade åstadkommit mycket inom akustisk partikelseparation före 1993, men det året presenterade Mandralis och Feke, den första väl fungerande kontinuerliga separa-

51
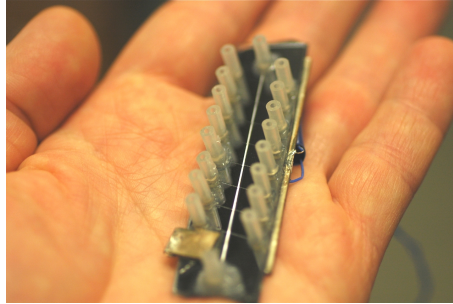
Figur 7.2: Ett laboratorium.

tionen av partiklar i ett stående vågfält [16]. De injicerade plastpartiklar genom en kanal vars dimension i höjdled var anpassad så att en stående våg kunde skapas mellan golv och tak, vinkelrätt mot flödesriktningen, se **Fig. 7.3**. Ljudvågorna skapas genom att koppla en växelspänning till ett så kallat piezokeramiskt element varpå mekaniska vibrationer uppstår och sprider sig i kaviteten. Under en passage genom kaviteten påverkas partiklarna, som inledningsvis är slumpmässigt fördelade i flödet, av en kraft som centrerar dem i höjdled så att de passerar ut genom det nedre av de två utloppen.
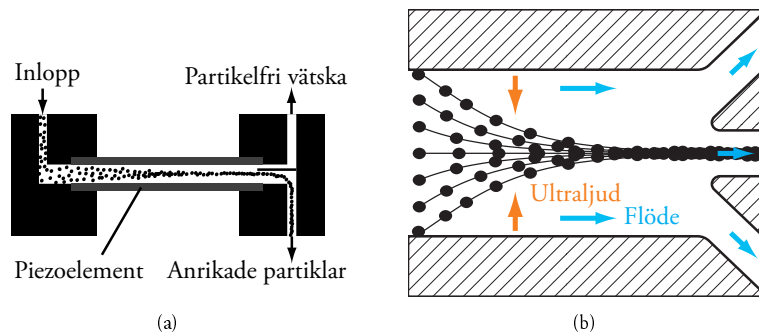
Figur 7.3: (a) Den första akustiska partikelseparatorn för kontinuerligt flödande partiklar. (b) Principskiss av den typ av partikelseparator som används i denna avhandling.

Nilsson, Petersson, Persson, Jönsson och Laurell presenterade sig för första gången 2002 med en, skulle det visa sig, mycket användbar variant av ovan nämnda akustiska halvvågsseparator, **Fig. 7.3(b)** [21]. Designen är enligt legenden sprungen ur ett misslyckat examensarbete där två studenter försökte använda ultraljud för att blanda runt vätskor i en mikrokanal. Mixningen uteblev, tvärt om så kunde man se att partiklar ansamlade sig i centrerade band utmed kanalens längdriktning.

Denna avhandling baserar sig på en uppsättning sådana plattformar. Några av dessa redovisas i den populärvetenskapliga sammanfattningen.

8

Populärvetenskaplig sammanfattning

Denna avhandling handlar om akustofores, dvs. om hur ultraljud kan användas för separation av celler och mikroskopiska partiklar i en ytterst smal flödeskanal. Separationen kan handla om att man vill separera en typ av celler från en annan, som till exempel när man letar efter s.k. cirkulerande tumörceller i blodprover från cancerpatienter. I ett annat fall så vill man automatisera hanteringen av prover i ett antikroppslaboratorium där man utvecklar framtidens mediciner.

Separationskanalerna tillverkas genom att man etsar in ett nätverk av kanaler i en skiva av kisel. Man försluter kanalen med en glasskiva och borrar hål för inlopp och utlopp av vätskor. På utsidan av chipet fäster man ett ljudalstrande s.k. piezokeramiskt element som kan vibrera med över 1 miljon svängningar per sekund. Vibrationerna sprider sig snabbt i chipet och det uppstår akustiska resonanser inuti flödeskanalerna, eftersom ljudet studsar fram och tillbaks mellan kanalväggarna. När celler eller mikropartiklar passerar kanalen exponeras de för ljudet och en akustisk kraft trycker dem in mot kanalens mittfåra. Eftersom rörelsen in mot mitten är olika snabb för olika typer av celler eller partiklar så kan man utnyttja de akustiska krafterna för att separera partiklar från varandra. I slutet av kanalen grenas flödet av i tre eller fler utlopp och de celler eller partiklar som rört sig snabbast in mot mitten kommer att hamna i det centrala utloppet medan de akustiskt sett långsamma kommer att passera ut genom något av de två sidoutloppen.

Som nämnts ovan har vi i ett av projekten tagit oss an uppgiften att leta efter cirkulerande tumörceller i blodprover. En cirkulerande tumörcell är, som namnet antyder, en cell från en cancertumör som på något sätt har hamnat i blodcirkulationen. Man är tämligen säker på att dessa celler är involverade i uppkomsten av metastaser hos cancersjuka, men man förstår ännu inte i detalj hur det går till. Vad som är säkert är, att ur blodprover från cancerpatienter har man lyckats isolera celler av samma typ som finns i tumören. Det finns dock ännu ingen teknik som har visat sig tillräckligt effektiv för att man skall

kunna vara säker på att isolera alla tumörceller i ett provrör. Vi har designat ett akustoforeschip som i modellexperiment har visat sig kunna separera cancerceller från blodceller. Dock återstår ännu en hel del arbete innan vi kan testa chipet på blodprover donerade från cancerpatienter. Om denna eller någon annan teknik visar sig effektiv kommer man i framtiden kunna individualisera och övervaka behandlingen av cancerpatienter bättre. Det har även spekulerats i att man kommer att kunna spåra cancer i ett tidigt skede endast genom att analysera ett blodprov. Noteras bör att det sistnämnda bygger på ett antagande om att det finns cirkulerande tumörceller i ett tidigt skede av sjukdomsutvecklingen, något som ingen i nuläget vet.

I ett annat projekt har vi använt akustofores för att automatisera sökandet efter antikroppar ur antikroppsbibliotek. Antikroppar är stora molekyler som finns naturligt i blodet som en del av immunförsvaret. När ett främmande föremål kommer in i blodet, t.ex. en viruspartikel, kommer antikroppar att fastna på ytan av föremålet och signalera till de vita blodkropparna att de ska äta upp viruspartikeln. Antikroppen kan bara fastna på mycket specifika platser på virusytan s.k. antigen, och det är den selektiva egenskapen som gör att man inom immunteknologin är intresserad av att använda antikroppar för att utveckla nya läkemedel. Genom att extrahera en uppsättning naturliga antikroppar från blodet hos ett djur och modifiera dem på biokemisk väg kan man skapa enormt variationsrika samlingar, så kallade antikroppsbibliotek, av syntetiska antikroppar som man kan använda för att utveckla nya läkemedel och behandlingsmetoder. Processen att ur denna stora samling antikroppar isolera en enskild antikroppsvariant som passar bäst för att fastna på en viss utvald antigen är mycket arbetsintensiv och innefattar många manuella moment. En vanlig metod är att man fäster antigenet, till vilken man vill hitta en antikropp, på ytan av mikrometerstora kulor. Kulorna blandas i ett provrör med antikroppsbiblioteket och antikropparna som passar specifikt till antigenet kommer att fastna på kulan medan andra antikroppar blir kvar i vätskan. Kulorna centrifugeras ner till botten av provröret och vätskan sugs bort och ersätts med ren vätska. På så sätt har man ur det enorma antikroppsbiblioteket lyckats isolera en uppsättning antikroppar som binder till just det antigen man utforskar. För att underlätta och automatisera processen att isolera antikroppar utvecklade vi ett akustoforeschip där mikropartiklar med antikroppar bundna till ytan kan separeras från ett antikroppsbibliotek genom att den akustiska kraften flyttar partiklarna i sidled då de passerar mikrokanalen. Sidledsförflyttningen innebär att partiklarna flyttar sig från den ursprungliga vätskan, in i ett parallellt flöde av ren vätska. I slutet av kanalen förgrenas flödena och partiklarna med selekterade antikroppar samlas upp i ett provrör.

För att bättre kunna förstå fysiken bakom akustofores startades ett samarbete med DTU i Köpenhamn. Vi har gemensamt utvecklat en metod för att karaktärisera den akustiska resonansen i en akustoforeskanal. Detta görs genom att analysera rörelsemönstret hos mikropartiklar som exponeras för ett akustiskt fält. Vi har bland annat studerat den akustiska resonansens utbredning längs kanalen, frekvensberoendet och temperaturberoendet. En av de viktigaste upptäckterna var just hur otroligt temperaturkänsliga de akustiska resonansmönstren är vilket har stor betydelse för systemets reproducerbarhet och precision, något som vi hade direkt nytta av i projektet med cirkulerande tumörceller.

Bibliography

[1] H. Bruus. *Theoretical Microfluidics*. Oxford University Press, Oxford, 2008.

[2] A. Kundt. Über eine neue art akustischer staubfiguren und über die anwendung derselben zur bestimmung der schallgeschwindigkeit in festen körpern und gasen. *Ann Phys Chem*, 127(4):497–523, 1866.

[3] A. Kundt and O. Lehman. Longitudinal vibrations and acoustic figures in cylindrical columns of liquids. *Ann Phys Chem*, 153, 1874.

[4] E. Chladni. *Entdeckungen über die Theorie des Klanges*. Bey Weidmanns erben und Reich, Leipzig, 1787.

[5] M. Faraday. On a peculiar class of acoustical figures; and on certain forms assumed by groups of particles upon vibrating elastic surfaces. *Phil Trans R Soc London*, 121:299–340, 1831.

[6] Lord Rayleigh. On the circulation of air observed in kundt's tubes, and on some allied acoustical problems. *Phil Trans R Soc London*, 175:1–21, 1884.

[7] L. V. King. On the acoustic radiation pressure on spheres. *P Roy Soc Lond A Mat*, 147(861):212–240, 1934.

[8] E. Klein. Absolute sound intensity in liquids by spherical torsion pendula. *J Acoust Soc Am*, 9:312–320, 1938.

[9] K. Yosioka and Y. Kawasima. Acoustic radiation pressure on a compressible sphere. *Acustica*, 5:167–173, 1955.

[10] L. P. Gorkov. On the forces acting on a small particle in an acoustical field in an ideal fluid. *Soviet Physics - Doklady*, 6(9):773–775, 1962.

[11] A. Doinikov. Acoustic radiation force on a spherical particle in a viscousheat-conducting fluid. i. general formula. *J Acoust Soc Am*, 101(2):713–721, 1996.

[12] M. Settnes and H. Bruus. On the forces acting on a small particle in an acoustical field in a viscous fluid. *Phys Rev E*, submitted:http://arxiv.org/abs/1110.6037, 2011.

[13] M. Dyson, B. Woodward, and J. B. Pond. Flow of red blood cells stopped by ultrasound. *Nature*, 232:572–573, 1971.

[14] N. V. Baker. Segregation and sedimentation of red blood cells in ultrasonic standing waves. *Nature*, 239:398–399, 1972.

[15] Z. I. Mandralis, D. L. Feke, and R. J. Adler. Transient response of fine particle suspensions to mild planar ultrasonic fields. *Fluid/Particle Sep J*, 3(3):3897–3905, 1990.

[16] Z. I. Mandralis and D. L. Feke. Continuous suspension fractionation using acoustic and divided-flow fields. *Chem Eng Sci*, 48(23):3897–3905, 1993.

[17] K. Yasuda, S. Umemura, and K. Takeda. Concentration and fractionation of small particles in liquid by ultrasound. *Jpn J Appl Phys*, 34(5B):2715–2720, 1995.

[18] J. J. Hawkes, D. Barrow, J. Cefai, and W. T. Coakley. A laminar flow expansion chamber facilitating downstream manipulation of particles concentrated using an ultrasonic standing wave. *Ultrasonics*, 36(8):901–903, 1998.

[19] J. J. Hawkes and W. T. Coakley. Force field particle filter, combining ultrasound standing waves and laminar flow. *Sensor Actuat B-Chem*, 75(3):213–222, 2001.

[20] N. R. Harris, M. Hill, S. Beeby, Y. Shen, N. M. White, J. J. Hawkes, and W. T. Coakley. A silicon microfluidic ultrasonic separator. *Sensor Actuat B-Chem*, 95(1-3):425–434, 2003.

[21] A. Nilsson, F. Petersson, H. W. Persson, H. Jönsson, and T. Laurell. Manipulation of suspended particles in a laminar flow. In Y. Baba *et al.*, editor, *Proc. MicroTAS 2002 Symposium, 3 - 7 November, Nara, Japan*, pages 751–752. Kluwer academic publishers, 2002.

[22] A. Nilsson, F. Petersson, H. Jönsson, and T. Laurell. Acoustic control of suspended particles in micro fluidic chips. *Lab Chip*, 4(2):131–135, 2004.

[23] F. Petersson, A. Nilsson, C. Holm, H. Jönsson, and T. Laurell. Separation of lipids from blood utilizing ultrasonic standing waves in microfluidic channels. *Analyst*, 129(10):938–943, 2004.

[24] F. Petersson, A. Nilsson, H. Jönsson, and T. Laurell. Carrier medium exchange through ultrasonic particle switching in microfluidic channels. *Anal Chem*, 77(5):1216–1221, 2005.

[25] F. Petersson, L. Åberg, A. M. Swärd-Nilsson, and T. Laurell. Free flow acousto-phoresis: microfluidic-based mode of particle and cell separation. *Anal Chem*, 79(14):5117–5123, 2007.

[26] J. Svennebring, O. Manneberg, and M. Wiklund. Temperature regulation during ultrasonic manipulation for long-term cell handling in a microfluidic chip. *J Micromech and Microeng*, 17(12):2469–2474, 2007.

[27] J. Dykes, A. Lenshof, I. B. Åstrand Grundström, T. Laurell, and S. Scheding. Efficient removal of platelets from peripheral blood progenitor cell products using a novel micro-chip based acoustophoretic platform. *PLoS ONE*, 6:e23074, 2011.

[28] O. Manneberg, M. Hagsäter, J. Svennebring, H. M. Hertz, J. P. Kutter, H. Bruus, and M. Wiklund. Spatial confinement of ultrasonic force fields in microfluidic channels. *Ultrasonics*, 49(1):112–119, 2009.

[29] J. D. Adams and H. T. Soh. Tunable acoustophoretic band-pass particle sorter. *Appl Phys Lett*, 97:064103, 2010.

[30] J. D. Adams, P. Thevoz, H. Bruus, and H. T. Soh. Integrated acoustic and magnetic separation in microfluidic channels. *Appl Phys Lett*, 95:254103, 2009.

[31] J. McCafferty, A. D. Griffiths, G. Winter, and D. J. Chiswell. Phage antibodies: filamentous phage displaying antibody variable domains. *Nature*, 348:552–554, 1990.

[32] J. J. Hawkes, R. W. Barber, D. R. Emerson, and W. T. Coakley. Continuous cell washing and mixing driven by an ultrasound standing wave within a microfluidic channel. *Lab Chip*, 4(5):446–452, 2004.

[33] B. Mostert, S. Sleijfer, J. A. Foekens, and J. W. Gratama. Circulating tumor cells (CTCs): detection methods and their clinical relevance in breast cancer. *Cancer Treat Rev*, 35(5):463–474, 2009.

[34] D. C. Danila, G. Heller, G. A. Gignac, R. Gonzalez-Espinoza, A. Anand, E. Tanaka, H. Lilja, L. Schwartz, S. Larson, M. Fleisher, and H. I. Scher. Circulating tumor cell number and prognosis in progressive castration-resistant prostate cancer. *Clin Cancer Res*, 13(23):7053–7058, 2007.

[35] W. J. Allard, J. Matera, M. C. Miller, M. Repollet, M. C. Connelly, C. Rao, A. G. Tibbe, J. W. Uhr, and L. W. Terstappen. Tumor cells circulate in the peripheral blood of all major carcinomas but not in healthy subjects or patients with nonmalignant diseases. *Clin Cancer Res*, 10(20):6897–6904, 2004.

[36] R. Königsberg, M. Gneist, D. Jahn-Kuch, G. Pfeiler, G. Hager, M. Hudec, C. Dittrich, and R. Zeillinger. Circulating tumor cells in metastatic colorectal cancer: efficacy and feasibility of different enrichment methods. *Cancer Lett*, 293:117–123, 2010.

[37] James Lighthill. *Waves in Fluids*. Cambridge University Press, 2002.

[38] A. D. Pierce. *Acoustics*. Acoustical Society of America, Woodbury, 1991.

[39] P. Tabeling. *Introduction to Microfluidics*. Oxford University Press, Oxford, 2005.

[40] G. Karniadakis, A. Beskok, and N. Aluru. *Microflows and Nanoflows: Fundamentals and Simulation*. Springer Science+Business Media, Inc., New York NY, 2005.

[41] N.-T. Nguyen and S. T. Wereley. *Fundamentals and Applications of Microfluidics*. Artech House, Norwood MA, second edition, 2006.

[42] J. Berthier and P. Silberzan. *Microfluidics for Biotechnology*. Artech House, Norwood MA, second edition, 2010.

[43] B. Kirby. *Micro- and Nanoscale Fluid Mechanics: Transport in Microfluidic Devices*. Cambridge University Press, New York, 2010.

[44] T. M. Squires and S. R. Quake. Microfluidics: Fluid physics at the nanoliter scale. *Rev Mod Phys*, 77:977–1026, 2005.

[45] I. Iranmanesh, R. Barnkob, H. Bruus, and M. Wiklund. Analysis of a tunable-angle wedge transducer for improved microchip acoustiphoresis. In *International congress of ultrasonics*, 2011.

[46] T. Hedberg. Modeling of ultrasonic fields in microfluidic separation systems. Master's thesis, Lund University, 2007.

[47] R. Barnkob. Acoustofluidics in microsystems: investigation of resonances. Master's thesis, Technical University of Denmark, www.nanotech.dtu.dk/microfluidics, 2009.

[48] R. Barnkob, P. Augustsson, T. Laurell, and H. Bruus. Measuring the local pressure amplitude in microchannel acoustophoresis. *Lab Chip*, 10(5):563–570, 2010.

[49] L. Mejling Andersen, A. Nysten, and M. Settnes. Forces acting on microparticles in acoustofluidic systems. Master's thesis, Technical University of Denmark, www.nanotech.dtu.dk/microfluidics, 2009.

[50] H. Bruus. Acoustofluidics 2: Perturbation theory and ultrasound resonance modes. *Lab Chip*, in press:(Tutorial Part 2), 2011.

[51] H. Bruus. Acoustofluidics 7: The acoustic radiation force on small particles. *Lab Chip*, in press:(Tutorial Part 7), 2011.

[52] M. F. Hamilton, Y. A. Ilinskii, and E. A. Zabolotskaya. Acoustic streaming generated by standing waves in two-dimensional channels of arbitrary width. *J Acoust Soc Am*, 113(1):153–160, 2003.

[53] P. Augustsson. Ultrasonic control of particles in microfluidic channels. Master's thesis, Lund University, 2006.

[54] R. J. Townsend, M. Hill, N. R. Harris, and N. M. White. Modelling of particle paths passing through an ultrasonic standing wave. *Ultrasonics*, 42(1-9):319–324, 2004.

[55] S. R. Springston, M. N. Myers, and J. C. Giddings. Continuous particle fractionation based on gravitational sedimentation in split-flow thin cells. *Anal Chem*, 59(2):344–350, 1987.

[56] D. A. Johnson and D. L. Feke. Methodology for fractionating suspended particles using ultrasonic standing wave and divided flow fields. *Separ Technol*, 5(4):251–258, 1995.

[57] C. Mikkelsen and H. Bruus. Microfluidic capturing-dynamics of paramagnetic bead suspensions. *Lab Chip*, 5(11):1293–1297, 2005.

[58] F. Petersson, A. Nilsson, C. Holm, H. Jönsson, and T. Laurell. Continuous separation of lipid particles from erythrocytes by means of laminar flow and acoustic standing wave forces. *Lab Chip*, 5(1):20–22, 2005.

[59] P. Augustsson, R. Barnkob, C. Grenvall, T. Deierborg, P. Brundin, H. Bruus, and T. Laurell. Measuring the acoustophoretic contrast factor of living cells in microchannels. In S. Verporte *et al.*, editor, *Proc. 14th MicroTAS, 3 - 7 October 2010, Groningen, The Netherlands*, pages 1337–1339. CBMS, 2010.

[60] R. Barnkob, P. Augustsson, C. Magnusson, H. Lilja, T. Laurell, and H. Bruus. Measuring density and compressibility of white blood cells and prostate cancer cells by microchannel acoustophoresis. In J.P. Landers *et al.*, editor, *Proc. 15th MicroTAS, 2 - 6 October 2011, Seattle (WA), USA*, pages 127–129. CBMS, 2011.

[61] S. H. Wang, L. P. Lee, and J. S. Lee. A linear relation between the compressibility and density of blood. *J Acoust Soc Am*, 109(1):390–396, 2001.

[62] M. A. H. Weiser and R. E. Apfel. Extension of acoustic levitation to include the study of micron-size particles in a more compressible host liquid. *J Acoust Soc Am*, 71(5):1261–1268, 1982.

[63] D. Hartono, Y. Liu, P. L. Tan, X. Y. S. Then, L.-Y. L. Yung, and K.-M. Lim. On-chip measurements of cell compressibility via acoustic radiation. *Lab Chip*, page DOI: 10.1039/C1LC20687G, 2011.

[64] C. Grenvall, P. Augustsson, J. Riis Folkenberg, and T. Laurell. Harmonic microchip acoustophoresis: A route to online raw milk sample precondition in protein and lipid content quality control. *Anal Chem*, 81(15):6195–6200, 2009.

[65] G. Goddard and G. Kaduchak. Ultrasonic particle concentration in a line-driven cylindrical tube. *J Acoust Soc Am*, 117(6):3440–3447, 2005.

[66] G. Goddard, J. C. Martin, S. W. Graves, and G. Kaduchak. Ultrasonic particle-concentration for sheathless focusing of particles for analysis in a flow cytometer. *Cytometry A*, 69A:66–74, 2006.

[67] C. Grenvall, P. Augustsson, F. Petersson, and T. Laurell. Fluorescent activated cell sorter using ultrasound standing waves in microchannels. In J.-L. Viovy *et al.*, editor, *Proc. 11th MicroTAS, 7 - 11 October 2007, Paris, France*, pages 1813–1815. CBMS, 2007.

[68] C. Grenvall, P. Augustsson, and T. Laurell. Reduced particle size dispersion in free flow acoustophoresis (ffa) using 2d acoustic prefocusing. In K. Song Kim *et al.*, editor, *Proc. 13th MicroTAS, 2009, Jeju, Korea*, pages 776–778. CBMS, 2009.

[69] S. M. Hagsäter, T. G. Jensen, H. Bruus, and J. P. Kutter. Acoustic resonances in microfluidic chips: full-image micro-PIV experiments and numerical simulations. *Lab Chip*, 7(10):1336–1344, 2007.

[70] J. G. Santiago, S. T. Wereley, C. D. Meinhart, D. J. Beebe, and R. J. Adrian. A particle image velocimetry system for microfluidics. *Exp Fluids*, 25(4):316–319, 1998.

[71] R. J. Adrian. Twenty years of particle image velocimetry. *Exp Fluids*, 39(2):159–169, 2005.

[72] M. Raffel, C. E. Willert, S. T. Wereley, and J. Kompenhans. *Particle Image Velocimetry*. Springer, 2007.

[73] R. Lindken, M. Rossi, S. Grosse, and J. Westerweel. Micro-particle image velocimetry (μ piv): Recent developments, applications, and guidelines. *Lab Chip*, 9(17):2551–2567, 2009.

[74] S. T. Wereley and C. D. Meinhart. Recent advances in micro-particle image velocimetry. *Annu Rev Fluid Mech*, 42:557–576, 2010.

[75] Oxford University Press and Oxford. *A Dictionary of Scientists*. Oxford University Press, USA, updated & abridged edition, 1999.